Geophysical Journal International

Geophys. J. Int. (2011) **184,** 1037–1057 doi: 10.1111/j.1365-246X.2010.04910.x

Segmented African lithosphere beneath the Anatolian region inferred from teleseismic *P*-wave tomography

C. Berk Biryol,[1] Susan L. Beck,[1] George Zandt[1] and A. Arda Özacar[2]

[1] *Department of Geosciences, University of Arizona, Tucson, AZ, USA. E-mail: cbbiryol@email.arizona.edu*
[2] *Geological Engineering Department, Middle East Technical University, Ankara, Turkey*

Accepted 2010 November 29. Received 2010 November 19; in original form 2010 July 9

SUMMARY

Lithospheric deformation throughout Anatolia, a part of the Alpine–Himalayan orogenic belt, is controlled mainly by collision-related tectonic escape of the Anatolian Plate and subduction roll-back along the Aegean Subduction Zone. We study the deeper lithosphere and mantle structure of Anatolia using teleseismic, finite-frequency, *P*-wave traveltime tomography. We use data from several temporary and permanent seismic networks deployed in the region. Approximately 34 000 *P*-wave relative traveltime residuals, measured in multiple frequency bands, are inverted using approximate finite-frequency sensitivity kernels. Our tomograms reveal segmented fast seismic anomalies beneath Anatolia that corresponds to the subducted portion of the African lithosphere along the Cyprean and the Aegean trenches. We identify these anomalies as the subducted Aegean and the Cyprus slabs that are separated from each other by a gap as wide as 300 km beneath Western Anatolia. This gap is occupied by slow velocity perturbations that we interpret as hot upwelling asthenosphere. The eastern termination of the subducting African lithosphere is located near the transition from central Anatolia to the Eastern Anatolian Plateau or Arabian–Eurasian collision front that is underlain by large volumes of hot, underplating asthenosphere marked by slow velocity perturbations. Our tomograms also show fast velocity perturbations at shallow depths beneath northwestern Anatolia that sharply terminates towards the south at the North Anatolian Fault Zone (NAFZ). The associated velocity contrast across the NAFZ persists down to a depth of 100–150 km. Hence, our study is the first to investigate and interpret the vertical extent of deformation along this nascent transform plate boundary.

Overall, the resolved upper-mantle structure of Anatolia is directly related with the geology and tectonic features observed at the surface of the Anatolian Plate and suggest that the segmented nature of the subducted African lithosphere plays an important role in the evolution of Anatolia and distribution of its tectonic provinces.

Key words: Mantle processes; Seismic tomography; Transform faults; Subduction zone processes; Continental margins: convergent; Dynamics of lithosphere and mantle.

1 INTRODUCTION

Anatolia is a part of the Alpine–Himalayan orogenic belt, formed by discrete coalesced pieces of continental lithosphere amalgamated during the Cenozoic closure and terminal suturing of the northern and southern branches of the Neotethys Ocean (Şengör & Yılmaz 1981; Görür *et al.* 1984; Robertson & Dixon 1984; Şengör *et al.* 1984). The recent tectonics of the region is controlled by northward collision of the Arabian Plate and westward extrusion of the Anatolian Plate along the North Anatolian and East Anatolian Fault Zones (NAFZ and EAFZ, respectively). In addition, the northward subduction of African lithosphere along the southwestward retreating Aegean trench and obstructed Cyprean trench plays an important role in the tectonic development of the region (Bozkurt 2001, Fig. 1).

The processes of collision-related tectonic escape of the Anatolian Plate and the subduction roll-back taking place along the Aegean Subduction Zone (ASZ) resulted in different styles of lithospheric deformation throughout the region. Based on these deformation styles, the Anatolian region can be subdivided into four tectonic provinces as described by Şengör *et al.* (1985): the East Anatolian contractional, the North Anatolian, the Central Anatolian and the West Anatolian extensional provinces (Fig. 1).

In the framework of these provinces, the Aegean and the Cyprean trenches play a key role in the distribution of the tectonic regimes within the Eastern Mediterranean region. Studies showed that the

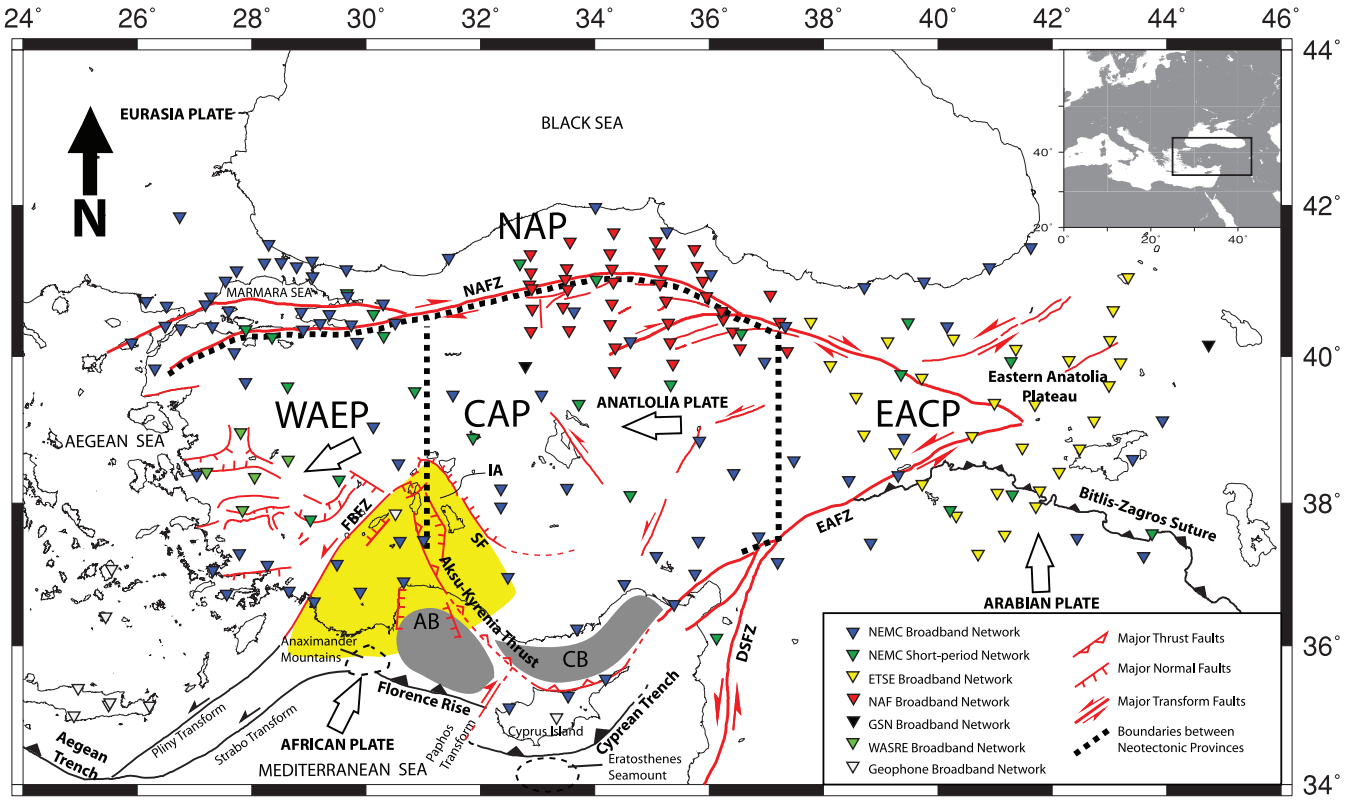

Figure 1. Location map of the study area and the major tectonic and geological features of the region. The distribution of the seismic stations used in our study is also shown. The thick white arrows shows the motion directions of the associated plates with respect to Eurasia (McClusky *et al.* 2003). The approximate boundaries between zones of different tectonic deformation styles (different tectonic provinces) are indicated with thick dashed lines. These provinces are EACP, Eastern Anatolian Contractional Province; CAP, Central Anatolian Province; WAEP, Western Anatolian Extensional Province; NAP, North Anatolian Province (modified from Barka & Reilinger 1997; Bozkurt 2001). The yellow region shows the Isparta Angle (IA) and the grey regions show the Antalya and Cilicia Basins (AB and CB, respectively). NAFZ, North Anatolian Fault Zone; EAFZ, East Anatolian Fault Zone; DSFZ, Dead Sea Fault Zone; FBFZ, Fethiye-Burdur Fault Zone; SF, Sultandağ Fault.

Cyprean trench is less active in terms of seismicity compared to the Aegean trench (Wdowinski *et al.* 2006). Based on the large-scale tomographic model of Piromallo & Morelli (2003), Faccenna *et al.* (2006) described the subducting portion of the African lithosphere between southwestern Anatolia and the Cyprus Island as less well defined and vertically discontinuous. Faccenna *et al.* (2006) further observed that the seismic velocity anomaly related with this slab-like structure disappears completely east of Cyprus. Many studies point out that subduction along the Cyprus section of the trench is influenced by the collision of the Eratosthenes Seamount (a part of the African promontory) with the Cyprean trench (Robertson 1994, 1998; Robertson & Grasso 1995; Glover & Robertson 1998, Fig. 1).

To investigate the relationship between the distribution of the major geological and tectonic features associated with the tectonic provinces and the upper-mantle structure beneath Anatolia, we carried out seismic tomography analysis in this region. Our aim in this study was to provide better constraints on the structure of the subducting African lithosphere along both the Aegean trench and particularly the Cyprean trench.

1.1 Tectonic setting

The East Anatolian Contractional Province (EACP) is characterized by N–S convergence between the Arabian Plate to the south and the Eurasian Plate to the north. Following the closure of the southern branch of Neotethys during the middle Miocene N–S contraction in the region gave way to the formation and widespread distribution of left- and right-lateral conjugate strike-slip faults during the early Pliocene (∼5 Ma). Recent geophysical investigations in the region revealed thin crust and mantle lithosphere beneath the Eastern Anatolian Plateau (EAP, Fig. 1, Türkelli *et al.* 1996; Sandvol *et al.* 1998; Gök *et al.* 2000; Al-Lazki *et al.* 2003; Zor *et al.* 2003; Angus *et al.* 2006; Özacar *et al.* 2008, 2010b). Based on these observations and geochemical analysis of igneous rocks exposed in the EAP, it has been proposed that the uplift of the plateau is associated with the steepening and break-off of the northward subducting Arabian lithosphere (∼11 Ma). Consequently, the upwelling hot asthenosphere replaced the slab, giving way to recent volcanism and supporting the 2-km-high plateau (Keskin 2003; Şengör *et al.* 2003). This event also marks a dramatic change in the stress field throughout the EAP, as suggested by Koçyiğit *et al.* (2001) and Örgülü *et al.* (2003). Teleseismic tomography studies by Lei & Zhao (2007) indicated the presence of a detached slab located at depths as shallow as 180 km beneath the EAP. However, a more recent teleseismic tomography study by Zor (2008) indicated the presence of the detached slab at ∼600 km depth.

The North Anatolian Province (NAP) is the area located to the north of the NAFZ and is characterized by nearly E–W striking dextral strike-slip faults. The basement of the Northern Anatolian crust is relatively old, with variably metamorphosed, intensely deformed

and imbricated Precambrian to Late Palaeozoic rocks associated with the closure of Paleotethys (Aydın *et al.* 1986; Okay 1996; Görür *et al.* 1997; Dean *et al.* 2000). It is commonly agreed that the NAFZ follows the Neotethyan suture along the northern margin of the Anatolian Plate (Koçyiğit, 1996; Bozkurt 2001; Şengör *et al.* 2005). There are many studies on the age and the total offset of the dextral NAFZ. The latest studies indicates that NAFZ is fairly young (∼5–7 Ma) and accommodates offsets in the range of ∼25–85 km along its different segments (Koçyiğit 1991; Bozkurt & Koçyiğit 1996; Barka *et al.* 2000; Bozkurt 2001; Şengör *et al.* 2005). Several geophysical studies from the western NAP around the Marmara Sea (Fig. 1) reported crustal thickness estimates ranging between 25 and 30 km around the Marmara Sea (Gürbüz & Üçer 1980; Laigle *et al.* 2008; Becel *et al.* 2009). Karahan *et al.* (2001) reported crustal thickness estimates of 39 km from the eastern Marmara region. In a recent study, Özacar *et al.* (2010a) reported crustal thicknesses in the order of 35–40 km for the central NAP. Unlike the EAP and the EACP, the deeper structure of the remaining parts of the NAP is not well constrained due to the lack of geophysical investigations.

The Central Anatolian Province (CAP) is a wedge-like region that is bounded by the NAFZ to the north and EAFZ to the southeast, and that extrudes westward along these structures (Fig. 1). The central part of this region is characterized by generally SW–NE striking, widely spaced, oblique-slip faults with dextral and sinistral components. Some of these structures are thought to be related to earlier deformation phases that were reactivated due to the N–S convergence between the African and Anatolian Plates and the anticlockwise rotation of the Anatolian block (Şengör *et al.* 1985; Reilinger *et al.* 1997; Bozkurt 2001; Taymaz *et al.* 2007a,b). The presence of diffuse fault zones in the central part of this province manifests itself with a flatter topography compared to Western Anatolian Extensional Province and EACP. This region is also characterized by ∼13 Ma to Recent post-collision related volcanism that was followed by emplacement of several stratovolcanoes (Pasquare *et al.* 1988; Notsu *et al.* 1995). Recently, the northern and central parts of this province were studied in detail using P_n tomography. Results indicate the presence of anomalously slow P_n velocities ($<$7.8 km s^{-1}) located at the eastern edge of this province (Gans *et al.* 2009). The southwestern edge of this province is known as the 'Isparta Angle' (IA on Fig. 1).

The Isparta Angle is a tectonically complex zone consisting of SE- and SW-vergent allochthons that were emplaced during multiple tectonic phases between the Late Cretaceous and the Late Miocene (Şengör & Yılmaz 1981; Robertson *et al.* 2003; Robertson *et al.* 2009). This zone is bounded by the NW–SE striking Sultandağ Fault (SF) to the east (Boray *et al.* 1985) and transtensional left-lateral NE–SW trending Fethiye-Burdur Fault Zone (FBFZ) to the west (Dumont *et al.* 1979; Taymaz & Price 1992; Price & Scott 1994, Fig. 1). The southernmost, offshore part of the Isparta angle is marked by the Anaximander Mountains. This region of pronounced sea floor relief with an anticlinal core is a part of the Anatolian Plate and is located at the cusp where the Aegean and western Cyprus trenches (Florence Rise) meet (Zitter *et al.* 2003; ten Veen *et al.* 2004, Fig. 1). In addition to these structures, the complexity of the region is further accentuated by the presence of the Late Pliocene–Recent Aksu-Kyrenia thrust at the centre of the Isparta Angle (McCallum & Robertson 1995; Poisson *et al.* 2003, Fig. 1); this marks the latest change in tectonic translation directions within this zone (Poisson *et al.* 2003). The region of the Isparta Angle hosts several basin bounding grabens, half-grabens and transtensional faults of various sizes (ten Veen *et al.* 2004; Alçiçek *et al.* 2005; Verhaert *et al.* 2006, Fig. 1). In the south, the offshore segment of the Aksu fault controls the NE margin of the Antalya forearc basin on the westside and the southern margin of the Cilicia forearc basin on the eastside (Aksu *et al.* 2005; İşler *et al.* 2005, Fig. 1). Recent onshore and offshore analysis of the structures and sediments hosted by these basins documented a change in stress field in the region during the latest phase of deformation.

The northern tip of the Isparta angle defines the boundary between the Western Anatolia Extensional Province (WAEP) and the Central Anatolia Province (Barka & Reilinger 1997; Glover & Robertson 1998; Bozkurt 2001, Fig. 1). The Western Anatolia Province is characterized by N–S extension and related formation of grabens bounded by roughly E–W striking normal faults (Taymaz *et al.* 1991; Jackson *et al.* 1992; Jackson 1994). The age and cause of the crustal extension in Aegean region is a subject of ongoing debate. Proposed explanations include tectonic escape (Dewey & Şengör 1979; Şengör 1979; Şengör *et al.* 1985; Görür *et al.* 1995), subduction roll-back (Mckenzie 1978; Le Pichon & Angelier 1979) and orogenic collapse (Seyitoğlu & Scott 1991; Seyitoğlu *et al.* 1992). The tectonic escape model suggests that the extension in the west is controlled by the westward extrusion of the Anatolia Plate along the NAFZ and EAFZ since 12 Ma (Bozkurt 2001, Fig. 1). The subduction roll-back model suggests that SW retreat of the Aegean trench results in backarc extension in Aegean region and Western Anatolia (Fig. 1). The orogenic collapse model proposes that the extension is due to the collapse and thinning of the thickened crust following the closure of the Neotethys ocean. The controversial ages for the extension ranges between 5 and 60 Ma depending on the controlling mechanism invoked (Bozkurt 2001). Several studies on the crustal seismic properties of the WAEP indicated crustal thicknesses ranging between 28 and 35 km (Kalafat *et al.* 1987; Saunders *et al.* 1998; Sodoudi *et al.* 2006; Zhu *et al.* 2006). Results of regional seismic tomography indicate the presence of the steeply dipping Eastern Mediterranean lithosphere underneath the Aegean region, favouring the idea that subduction roll-back plays an important role in the evolution of the region (Spakman *et al.* 1988; Faccenna *et al.* 2003; Piromallo & Morelli 2003; Faccenna *et al.* 2006). The central part of this province is characterized by Late Miocene and Pliocene volcanism (Yılmaz 1990; Delaloye & Bingöl 2000; Yılmaz *et al.* 2001). Recent geochemical studies showed that the evolution of these volcanics could be associated with a vertical tear in the subducting Mediterranean lithosphere (de Boorder *et al.* 1998; Tokçaer *et al.* 2005; Dilek & Altunkaynak 2009; Dilek & Sandvol 2009).

2 DATA AND METHOD

Seismic tomography is an important tool in investigating the mantle structure beneath an array of seismic stations. The mantle structure beneath the Mediterranean region has been studied by Spakman (1985), Bijwaard *et al.* (1998) and Piromallo & Morelli (2003) using seismic tomography. These studies covered broad regions and hence, had limitations in resolving finer-scale structures. The recent improvements in the geographical coverage of National Earthquake Monitoring Center (NEMC) seismographic network of Turkey (Kalafat *et al.* 2008) and several temporary seismic deployments have made it possible to improve the resolution and quality of the seismic studies for the Anatolia region. We studied a smaller part of the Eastern Mediterranean region at a finer scale using teleseismic *P*-wave tomography with finite-frequency approximation (Fig. 1). Although the narrower geographical span of the studied region limits the maximum depth for the resolvable structures, we

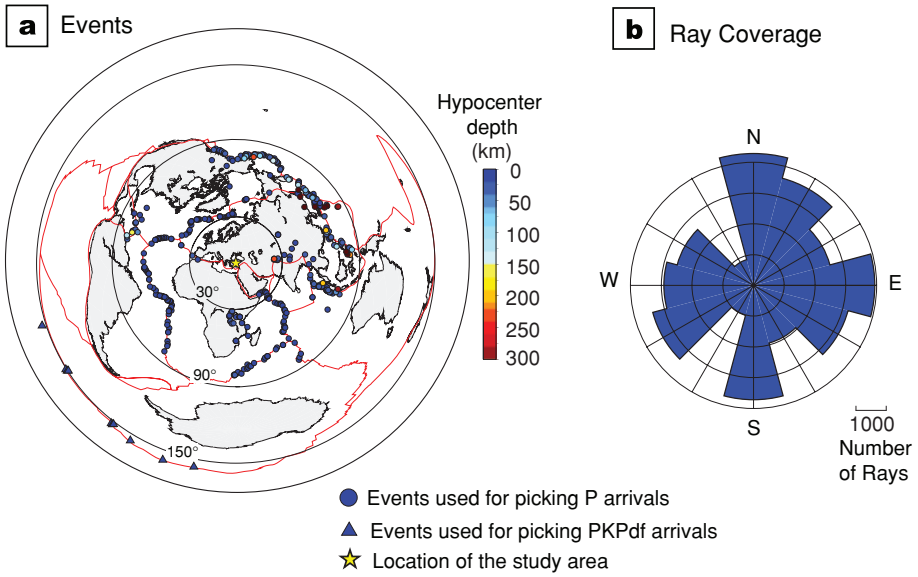

Figure 2. (a) Global distribution of the teleseismic events used in our study. (b) The backazimuthal coverage of all the arrivals (rays) picked.

can get finer resolution at shallower depths when compared to larger regional studies.

2.1 Data

The traveltime data that we have used in our analysis comes from 201 broadband and short-period seismic stations belonging to multiple seismographic networks operated in the region between 1999 and 2009. These networks are the National Earthquake Monitoring Center network (NEMC) (both short period and broadband deployments) (Kalafat *et al.* 2008), Global Seismographic Network (GSN), Eastern Turkey Passive Seismic Experiment (ETSE) (Türkelli *et al.* 2003), Geophone (GE), Western Anatolia Seismic Recording Experiment (WASRE) (Zhu *et al.* 2006) and our North Anatolian Fault passive seismic experiment network (NAF) (Gans *et al.* 2009, Fig. 1).

We used arrivaltime data from 409 teleseismic events with magnitudes $M_w > 5.0$ located at distances of 30–90° for direct P phases and 155–180° for PKPdf phases (Fig. 2a). We used the multichannel cross-correlation technique of Pavlis & Vernon (2010) for picking arrivals and calculated residual times with respect to IASP91. A total of 33 771 direct P and 219 PKPdf phases were picked on vertical components of broadband records in three frequency bands, to incorporate the measured traveltime residuals in a finite-frequency approximation. The passband filters that we used have corner frequencies of 0.2–0.8 Hz (short period), 0.1–0.4 Hz (intermediate period) and 0.04–0.16 Hz (long period) for broadband records. The picks associated with the short, intermediate and long period bands constitute 34, 36 and 27 per cent of the entire data set, respectively. The data from short-period stations are filtered only with a passband filter with corner frequencies 0.5–1.5 Hz and this subset constitutes only 3 per cent of the entire data set due to the lower quality of the teleseismic records. To avoid any directional bias in our results, we optimized the backazimuthal distribution of the observed residuals (Fig. 2b). The measured traveltime residuals were then demeaned for each event to obtain the relative traveltime residuals. The rms of the observed raw relative residuals is 0.56 s (also see Appendix A1, in the Supporting Information, for distribution of relative traveltime residuals). This is in agreement with the rms values for individual frequency bands that are all within 0.54–0.58 s.

Ray theory is used to calculate traveltime corrections for the observed relative traveltime residuals to account for crustal heterogeneities (Schmandt & Humphreys 2010). We incorporated crustal thickness and velocity estimates from several deep seismic sounding studies and from receiver function analysis for the region (Gürbüz & Üçer 1980; Kalafat *et al.* 1987; Gürbüz & Evans 1991; Türkelli *et al.* 1996; Sandvol *et al.* 1998; Saunders *et al.* 1998; Karahan *et al.* 2001; Zor *et al.* 2003; Sodoudi *et al.* 2006; Zhu *et al.* 2006; Laigle *et al.* 2008; Becel *et al.* 2009; Özacar *et al.* 2010a,b) to calculate correction times. The rms for these crustal corrections is 0.08 and after the corrections the rms of the relative traveltime residuals is 0.55, which is nearly the same value as the rms before the crustal corrections. This might be due to the lack of a direct correlation between observed traveltime residuals and the crustal corrections. In addition, this also shows that the major part of the seismic-speed anomaly exists in the mantle.

2.2 Method

The seismic arrivals observed on seismic records have a finite-frequency band width and their traveltimes are sensitive to seismic speed variations within the volume surrounding the geometrical ray path (Woodward 1992; Marquering *et al.* 1999; Dahlen *et al.* 2000; Hung *et al.* 2000; Zhao *et al*. 2000). The seismic waves with different frequency contents have different Fresnel zone widths and thus they sample different volumes of medium surrounding the geometrical ray path.

In this study, we used the teleseismic tomography algorithm of Schmandt & Humphreys (2010), which incorporates the use of frequency dependent 3-D sensitivity kernels. The use of these kernels helps us to account for volumetric variations in wave speeds when calculating the velocity perturbations in the tomography model. The usage of sensitivities is limited to the first Fresnel zone. Born theoretical 'banana–doughnut' kernel approximation of Dahlen *et al.* (2000) is used to calculate these sensitivities. The sensitivity kernels are approximated as a function of the dominant period of the

seismic arrival, epicentral distance, distances normal to the ray path and along the ray path and ray centred azimuth. Details of this algorithm are explained in Schmandt & Humphreys (2010). We prefer this tomographic algorithm because it allows us to incorporate means of interpreting the frequency dependence of traveltime data, making better use of broadband records and it introduces an intrinsic smoothness constraint for tomography through the use of approximate sensitivity kernels (see Appendices C1, C2 and C3, in Supporting Information, for comparison of single-frequency and integrated three-band frequency tomographic models for our data set). In addition, the sensitivity kernel approximation used in this algorithm has a high computational efficiency.

Smoothing is applied on the approximated sensitivity kernels to account for geometrical ray location uncertainty normal to the ray and along the ray path. Gradient and norm damping are also used to regularize the inverse problem. The gradient damping algorithm incorporates variations of ray path-normal damping weights as a function of depth to account for the increasing angle of inclination of the mean ray path. Norm damping, on the other hand, attempts to obtain the model with smallest possible perturbations satisfying the traveltime data, while strongly down-weighting anomalies that are weakly sampled by the observed set of rays (Schmandt & Humphreys 2010). The inverse problem is solved using the LSQR method of Paige & Saunders (1982) with an objective of minimizing the least-squares misfit between calculated and observed data in an iterative sequence. We performed trade-off analysis between Euclidian model norm and variance reduction to determine the smoothing weight and the overall damping factor (Menke 1989). Indeed, our tests showed that the variation in variance reductions for inversions with slightly varying (± 1.0) damping and smoothing weights were small (see Appendix A4, in Supporting Information, for various smoothing/damping trade-off plots and Appendix B1 and B2 for comparison of results obtained using different smoothing/damping parameters). We obtained an rms of 0.1 for the residuals after the inversion with favoured values of damping (6) and smoothening (7), achieving a variance reduction of $\sim$81 per cent.

Even though crustal corrections are applied to the observed relative traveltime residuals, station terms are included for each station in the inversion to account for the small-scale local variations and errors in incorporated crustal thicknesses and velocities. The rms for these terms is $\sim$0.09, which is small compared to the rms of the entire data set (0.55), showing that these terms explain only a small fraction of the data. Indeed, strong damping is applied to station terms to avoid any absorption of mantle structure by these terms. We tested the case where no crustal traveltime corrections were applied to the raw data. In this case, we observed that the rms for the station static terms increased by $\sim$0.05. This indicates that the station static terms effectively accounts for the varying shallow structure in the study area.

Event terms are also calculated representing the adjustment of the mean arrivaltime for the set of stations that recorded each event (see Appendices A2 and A3, in Supporting Information, for distribution of station and event terms). Our data set is composed of traveltime data from patchwork of regional seismic networks some of which are not concurrent in time. This might introduce the problem of shifts in calculated mean traveltime residuals between these networks that were deployed at geographically different parts of the study area. However, both the incorporation of the event terms in the inversion and usage of data from long-operating, spatially well-distributed/enveloping networks such as NEMC and GSN (Fig. 1) help us to account for variations or shifts in mean velocity structure in different portions of the study area. The calculated rms for the event terms is $\sim$0.02, also small compared to the overall rms of the data set.

2.3 Model parametrization

The region that we studied covers an area approximately 1100 km (E–W) $\times$ 900 km (N–S) and our average station spacing is roughly 50 km (Fig. 1). This region is parametrized with an irregularly spaced 3-D rectangular grid that starts at 35 km depth and extends down to 655 km depth. The lateral node spacing at the top of this volume varies from 35 to 50 km, with denser spacing (35 km) present only at the central to outer central parts of the seismic array. Towards the edges of the modelled volume, the node spacing increases gradually up to 50 km to account for the effects of reduced resolution power at the edges (Fig. 3a). The vertical node spacing increases from 35 to 50 km with increasing depth. Similarly, the horizontal node spacing gradually increases from 35 to 48 km at the centre of the model (50 to 70 km at the edges) from the top of the model to the bottom (Fig. 3b). Such dilations in node spacing as a function of depth constitute a more efficient parametrization approach, as the Fresnel zone width increases with depth whereas the resolution decreases. Our parametrized model has a total of 41 808 nodes with 67 (latitudinal)-by-39 (longitudinal) nodes in 16 layers.

To estimate the resolving power of our inversion with our data set, we investigated our sampling of the model space. For this purpose, we calculated hit quality maps for each depth layer of our model space (Figs 4a–d). These normalized hit quality maps are based on density of sampling of each node in a given layer, where the quality is also a function of the backazimuthal distribution of the sampling rays. The function governing the assignment of hit quality index is custom-built based on the idea that better resolution in seismic tomography is provided by rays from various directions intersecting at high angles (Schmandt & Humphreys 2010) (see Appendix D, in Supporting Information, for a summary table). Thus, a quality of 1 indicates that the associated node is sampled by at least five rays from each of the four geographical quadrants (NE, SE, SW and NW) and a quality of 0 indicates that the associated node is not sampled. The maps in Fig. 4 show us that better node sampling is restricted to nodes located directly beneath the individual stations at shallower depths (Fig. 4a), particularly for the top layer (35 km depth), due to the near vertical incidence of teleseismic arrivals that cluster around the stations. Thus, the broad-scale resolution is poor for this top layer. Further, this layer compensates for the errors in crustal corrections and poorly constrained variations in upper mantle. Hence, in the following sections where we discuss and interpret the resolved perturbations in our model, we will ignore anomalies resolved in this layer. In deeper parts of the modelled volume, the 'good' hit quality regions spread out to cover almost the entire study region (Figs 4b and c). At the bottom of the model, however, due to the reduction in sampling density at the edges of the model, the better sampled portions are limited to the central parts of the study area (Fig. 4d). We also observe a persistent pattern of relatively lower qualities in central parts at shallower depths (Figs 4a and b), which is an artefact of wider station spacing in these portions of the study area.

In addition to the quality of sampling of model space, we investigated the resolution in our model area through synthetic tests. Our synthetic tests involve layers with 'checkerboard' type velocity anomalies embedded in a neutral background. With this setup, we aimed to place constraints on the lateral (Figs 5a–d) and

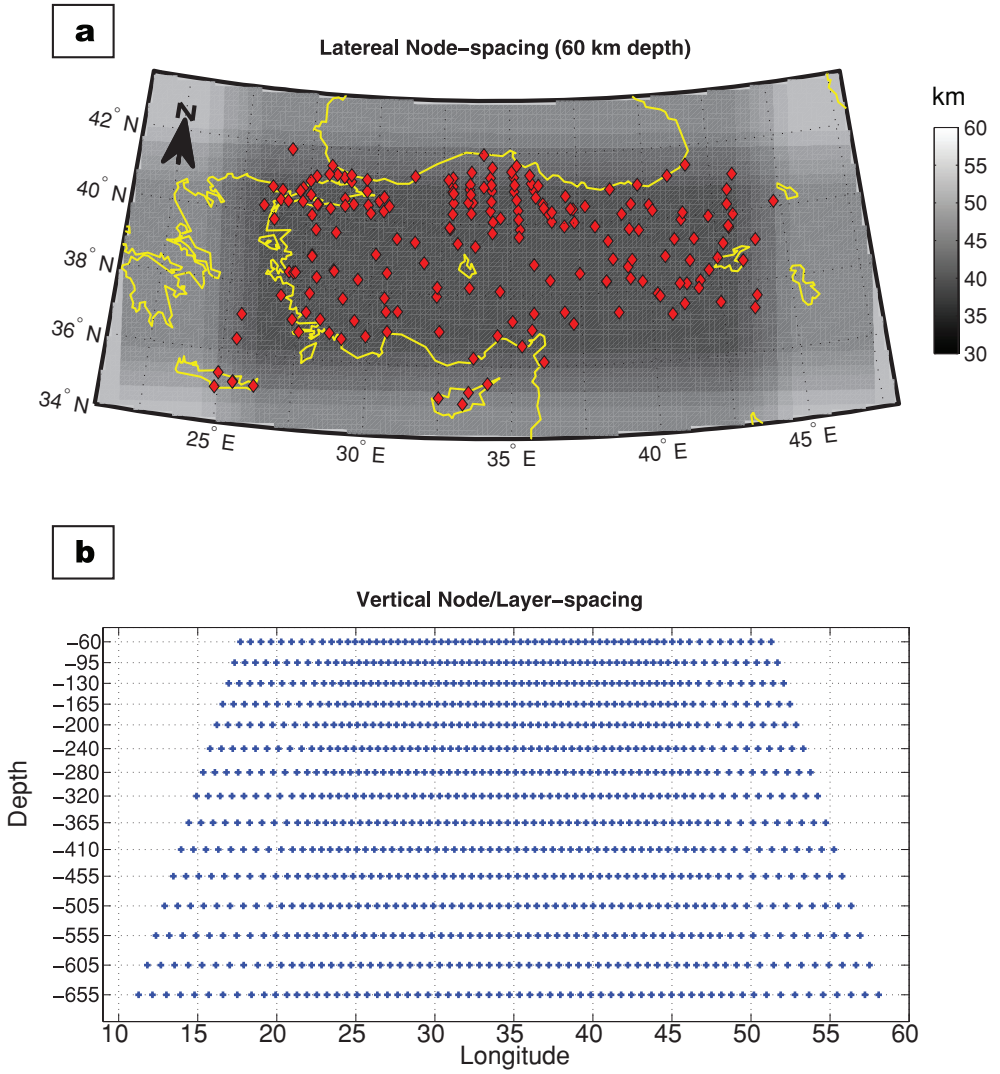

Figure 3. Node and layer spacing in our parametrized model. (a) Lateral node spacing at 60 km depth. (b) Layers and node spacing of our parametrized model on a verticle section along 39° latitude. Red diamonds shows the stations used in this study. Note the dilation in node spacing both towards the edges and with increasing depth.

vertical (Figs 5e and f) resolving power of our data set within the parametrized model. The volume of each perturbation in the layers of the checkerboard is defined by cube of two nodes (eight nodes total). Hence, the lateral and vertical extents of the individual anomalies vary as a function of position in the model and dilate with depth (Figs 5e and f) and towards the edges in accord with the dilation in node spacing within the model (Figs 3 and 5a–d). The intensities of the input perturbations are −3 and +3 per cent for slow and fast anomalies, respectively. These anomalies are separated by a cube of two nodes belonging to neutral background. Figs 5(a1–f1) shows the input synthetic structure and recovery of it after inversion (Figs 5a2–f2). The results of this test show that our resolution is good within the modelled volume and the study area. However, there is some amplitude decay and dilation in recovered perturbations due to minimum-length solution objective of the inversion procedure and subvertical incidence of teleseismic rays (Schmandt & Humphreys 2010). The inversion for the synthetic model achieved 60 per cent amplitude recovery of the input perturbations within the central parts of the model. In other words, a ±3.0 per cent perturbation in the input synthetic model is recovered as an anomaly of ±1.8 per cent within the resolved model. The peak amplitude recovery is 78 per cent. The losses in amplitude recovery during the inversion process are also a consequence of applied damping, smoothing and imperfect ray coverage. The vertical cross-sections also show some dilation and streaking of the recovered perturbations at the edges of the model due to sparse sampling. Although the reliability of these resolution tests is limited by the basic tomographic assumptions (i.e. isotropic and elastic mantle, well constrained ray locations at depth, accurate traveltime sensitivity kernels), the recovery of the pattern of perturbations in our resolution test indicates that we should be able to retrieve major upper-mantle structures (i.e. subducted lithosphere, plumes) using the data set at hand and the preferred parametrized model. In the following section, we will show results from additional resolution tests on specific features that emerge from the inversion.

It is important to keep in mind the results of the hit quality and checkerboard resolution tests when interpreting the modelled velocity perturbations, to avoid misinterpretation of anomalies located in regions of the model that are poorly resolved.

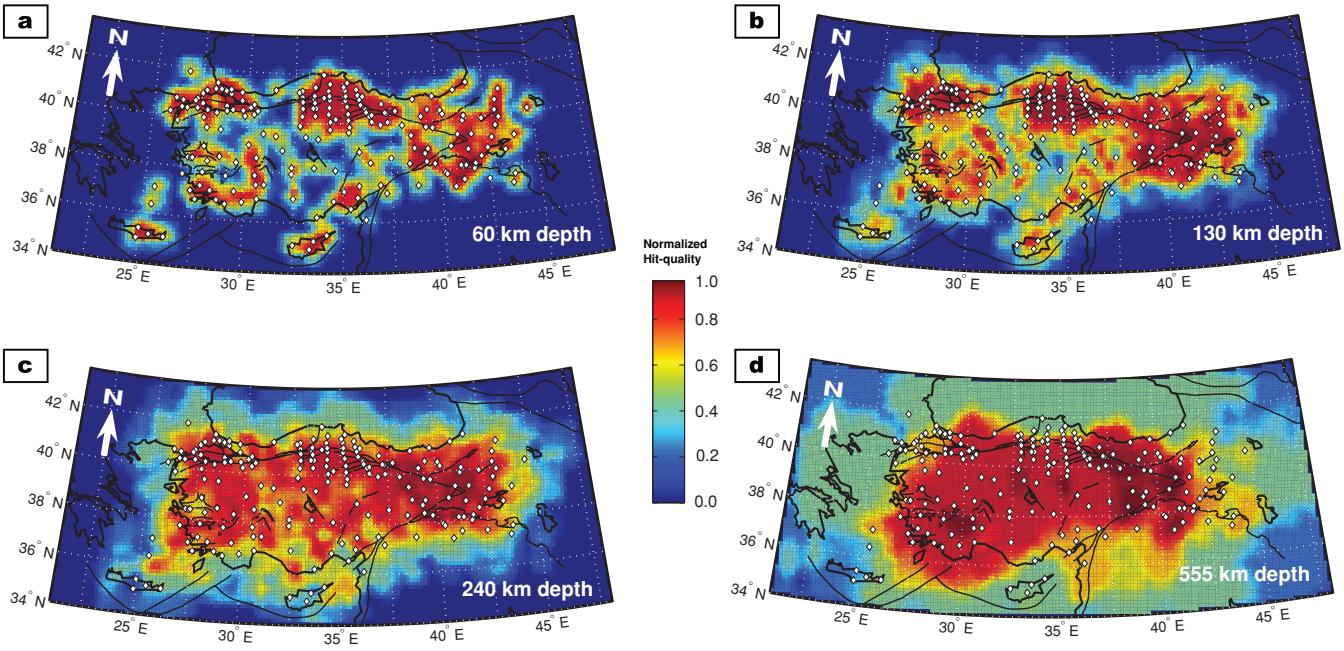

Figure 4. Normalized hit quality maps for our data set and parametrized model at various depths (plots a–d). Hit quality is based on the number and azimuthal distribution of rays. Red shading indicates good hit quality (1 on scale) and blue shading shows poor hit quality (0 on scale) for each node. White diamonds show the stations used in this study. Note that the spreading of the pattern of better hit qualities at deeper parts of the model.

3 RESULTS

3.1 Inversion

The data variance reduction is a common way of assessing the quality of the least squares solution to the tomographic inverse problem. As pointed out by Schmandt & Humphreys (2010), the overall variance reduction for the entire modelled volume gives a rather optimistic estimate owing to the fact that the setup of the forward problem heavily relies on the *a priori* assumptions (i.e. elastic, isotropic upper mantle, accurate ray locations) and the resolution of the solution shows variations throughout the modelled volume. As reported earlier, we obtained an overall data variance reduction of 81 per cent after the inversion. This indicates that the resultant model successfully explains most of the observed traveltime residuals. To test how successfully our resolved model explains the observed data, sampling the well-resolved parts, we adopted the same approach as Schmandt & Humphreys (2010), calculating the variance reduction for the portions of the model that are densely sampled and well resolved with a hit quality greater than 0.4 (i.e. rays from at least two backazimuth quadrants, excluding the top and bottom two layers). We obtained a variance reduction of 73 per cent for the 'high quality' parts of the resolved model. This shows that major portion of the observed traveltime residuals is explained within the well-sampled, well-resolved part of the model, although a minor portion of it is resolved as probable artificial heterogeneities at the poorly sampled, poorly constrained parts of the model (i.e. edges of the model), due to the objective of least squares inversion to minimize the length of the solution.

3.2 Tomograms

The resultant tomograms are shown in Figs 6 (map views) and 7 (cross-sections). In this section, we summarize the most prominent features of the resolved model and results of the realistic anomaly recovery analysis for testing the robustness of resolved features.

The most significant feature of the resultant model is the fast anomalies located to the north of the Aegean and the Cyprean trenches (Figs 6a–d and 7b and c). Overall, these fast anomalies have a mean perturbation of +1.7 per cent within the entire model and they shift in a northerly direction as a function of increasing depth. The general strikes of these anomalies are roughly NW on the Aegean side and E–W on the Cyprean side. The individual mean perturbations for Aegean and Cyprean anomalies above 450 km depth are +1.8 and +1.7 per cent, respectively. These two anomalies are separated by an N–S trending volume of slow perturbation located between 28° and 30° longitudes (Figs 6a–e and 7e and f). This slow anomaly has a mean perturbation of −1.4 per cent. We can also observe relatively fast anomalies (mean perturbation of +1.6 per cent) located to the north of the NAFZ at the western and eastern parts of the study area (Figs 6a and b). However, these anomalies are only observed at shallower depths (Figs 7c and d). The rest of the resultant model mostly contains scattered, small-scale and weaker slow velocity perturbations. The patterns of slow anomalies, however, are more persistent and continuous beneath eastern Anatolia (Figs 6a–d and 7d and e). The mean amplitude of the 'blob' of slow velocity anomaly beneath the EAP is −1.5 per cent. At depths below 500 km, the separated fast anomalies throughout the study area merge to form a continuous, WNW–ESE trending belt (mean perturbation of +1.7 per cent) that occupies the deeper, northern portions of the resolved model (Figs 6f–h and 7e).

The vertical slices (cross-sections) that cut across the study area show the dipping fast anomalies associated with the Aegean and the Cyprean trenches (Figs 7b and c). We also observe a clear eastern termination of the fast anomaly associated with the Cyprean trench at ∼34°E longitude (Fig. 7f). Along latitude 37°N, the slow anomaly that separates the Aegean and the Cyprean anomalies extend down to depths of 300 km (Fig. 7f). It becomes clear on the cross-sections

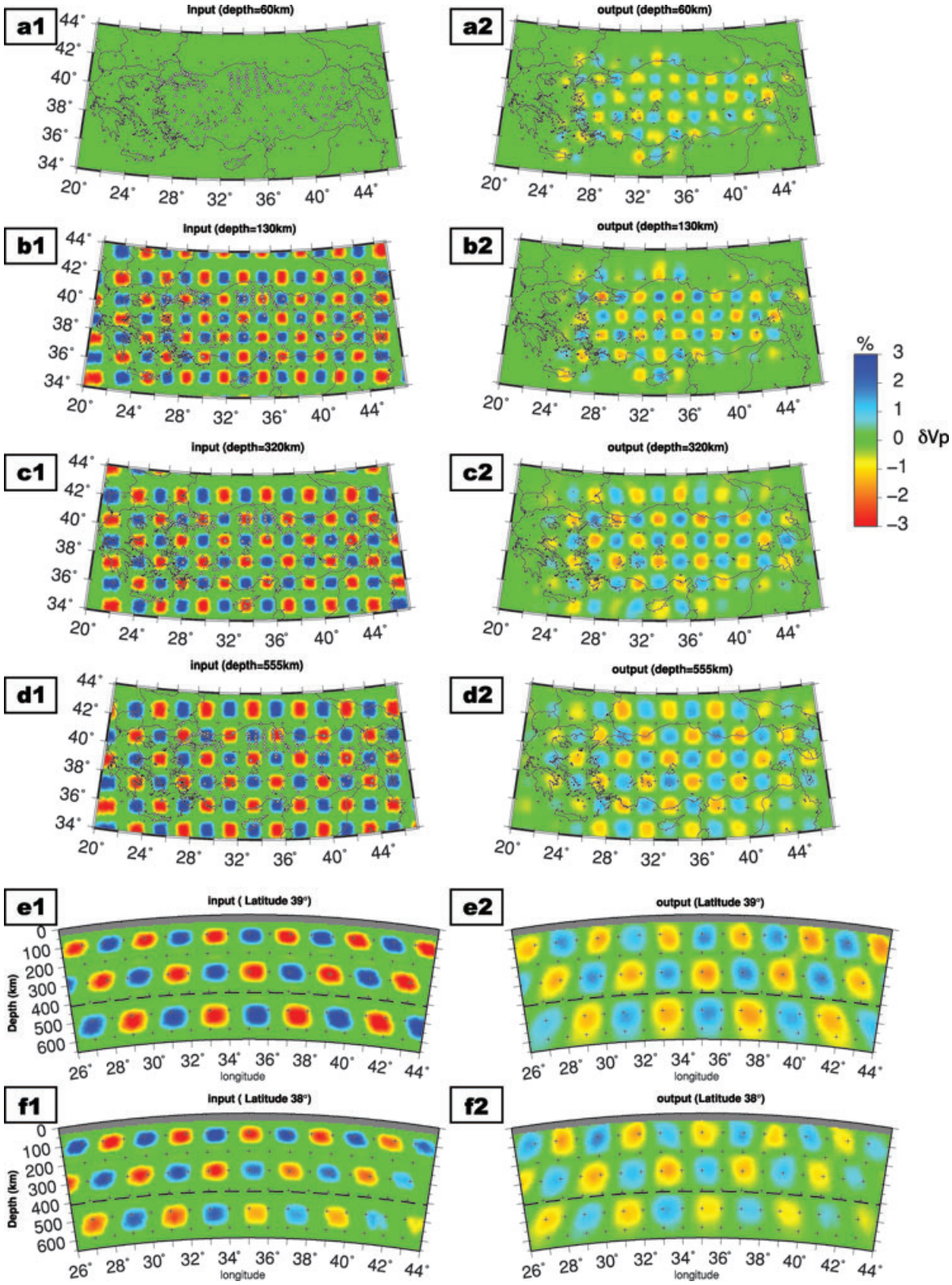

Figure 5. Results of the resolution tests presented in the form of horizontal slices (plots a–d) and vertical (latitudinal) cross-sections (plots e and f). The effects of vertical streaking can be seen at shallower depths (a1 and a2). The lateral resolution is generally good but there is some amplitude decay. The open triangles show the location of stations.

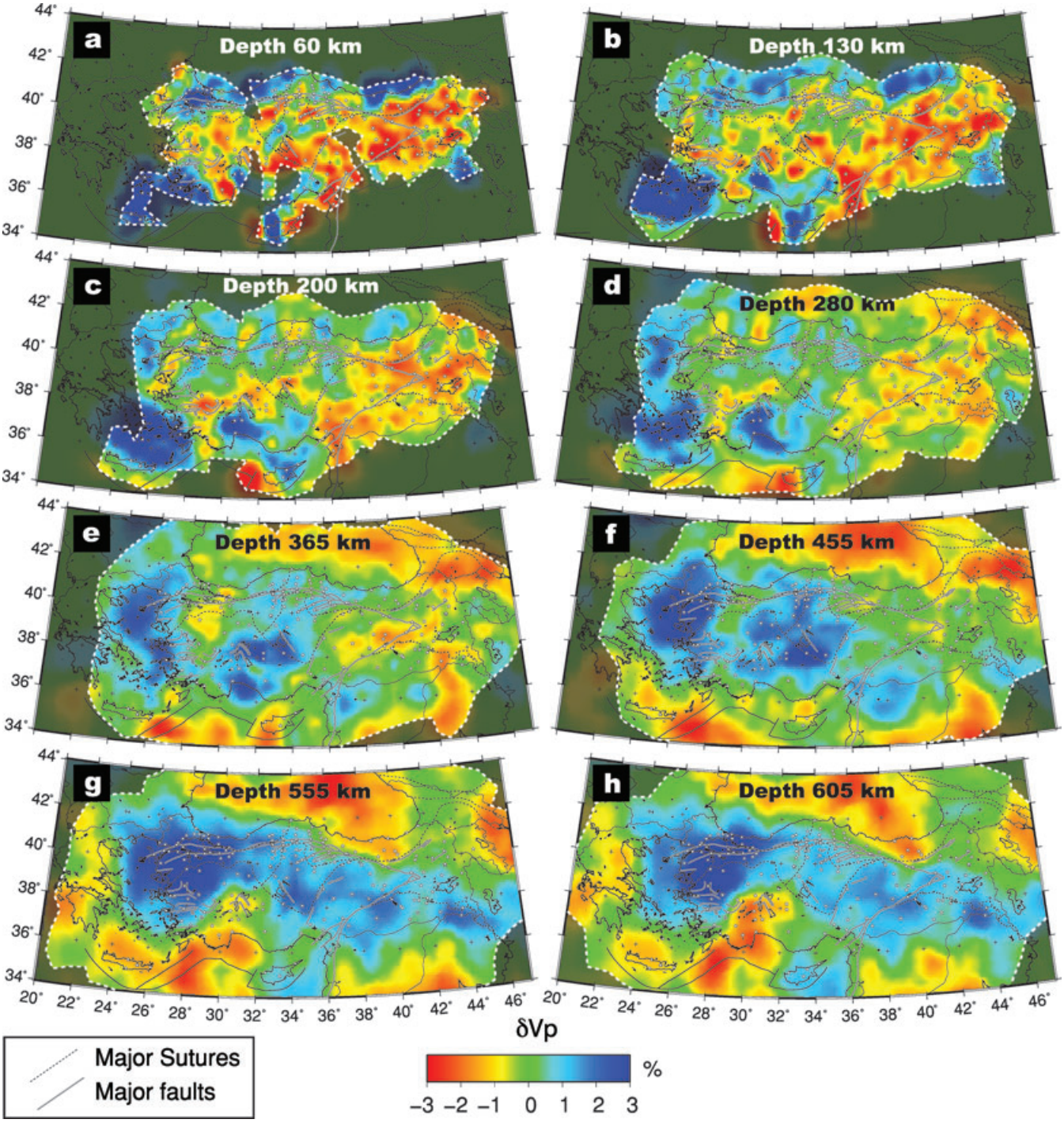

Figure 6. Horizontal slices at depths between 60 and 605 km (plots a–h) from the resultant tomography model. Open stars indicate the stations used in our study. The dark-shaded areas remaining outside of the white dashed line are poorly resolved portions of the model with hit qualities less than ∼0.2.

that these dipping fast anomalies merge at depths of ∼500 km and starts flattening out close to the bottom of the mantle transition zone (660 km) (Figs 6g and h and 7f). At the western part of the study area, the shallow fast anomalies located north of the NAFZ extend to depths of 100–150 km and terminate rather sharply at the downward projected trace of the NAFZ (Figs 6a and b). In the east, we observe consistent slow anomalies beneath the EAP that extend to depths of 300–400 km (Figs 6d and f). This is in agreement with the results from a recent teleseismic tomography study by Zor (2008). An earlier seismic tomography study by Lei & Zhao (2007) indicated the presence of a discontinuous, northward dipping fast anomaly in this region. Although our resolving power and hit quality is good in this portion of the study area, we do not observe such a fast structure. This discrepancy between the two tomographic models might be due to the differences in styles of sampling of the modelled volume of upper mantle. As it is mentioned earlier, we homogenized the backazimuthal ray coverage of our data set to avoid unwanted inversion artefacts such as smearing of imaged seismic anomalies along the ray paths. In their study, Lei & Zhao (2007) used rays from dominantly east backazimuths which might have introduced some

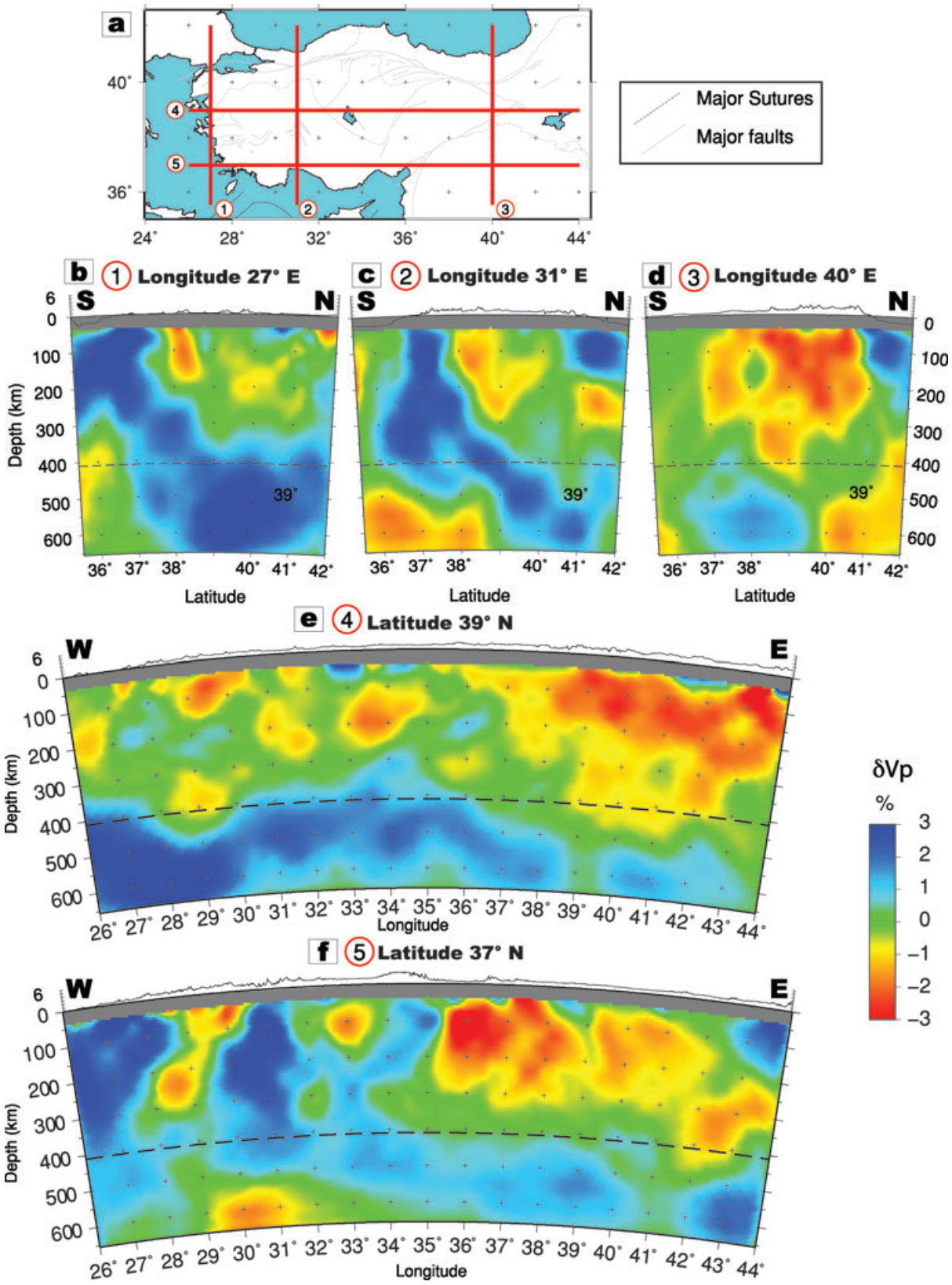

Figure 7. The resultant tomography model along various longitudinal (plots b–d) and latitudinal cross-sections (plots e and f). Topographic profiles are also shown at the top of each slice (with 10× vertical exaggeration). Numbered red lines on the map in the top panel (plot a) show locations of the cross-sections.

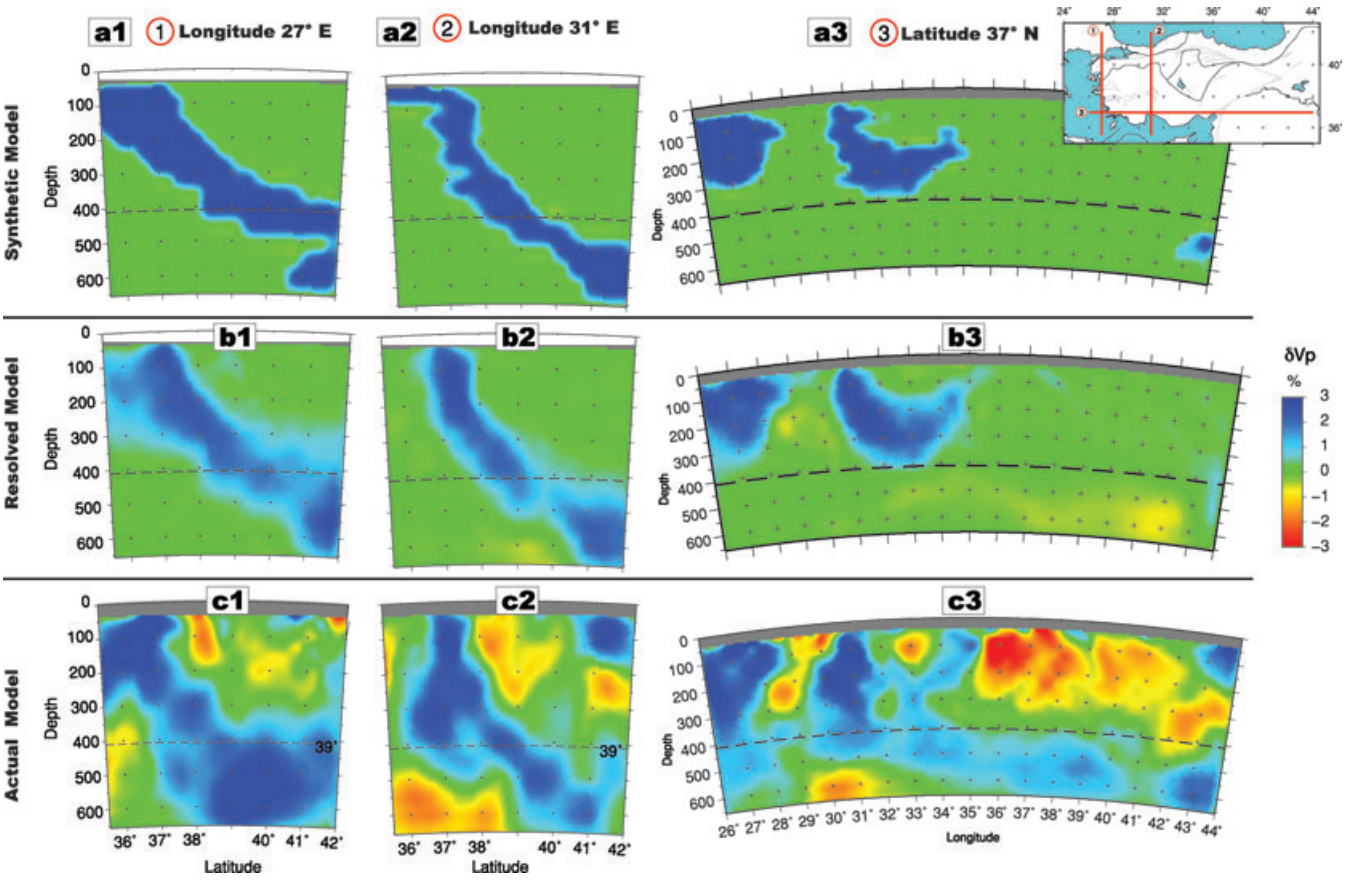

Figure 8. Results of realistic amplitude recovery tests on multiple cross-sections. Locations and section numbers are shown on the map at top right-hand corner. The top panel shows (plots a1–a3) input synthetic structure and the middle panel (plots b1–b3) shows the recovered anomalies after inversion. The bottom panel (plots c1–c3) shows the results from our tomographic model for comparison.

directional bias in resolved seismic anomalies in their tomographic model.

As indicated by our hit quality and synthetic tests, the resolution of our model is good in the central parts of our study region (Figs 4c and d and 5), although we lose resolution rapidly at the edges of our model. In this respect, the fast anomaly associated with the Aegean trench is less well resolved compared to the one for the Cyprean trench. The model edge related loss in resolution is also true for the central northern part of the study area and the southeastern corner, where station coverage is relatively sparse. Even though the sampling of the nodes and the associated hit qualities are strongly controlled by the station locations and station spacing at shallower depths (<100 km) (Fig. 4a), the station density is high enough at critical locations associated with major tectonic zones and structures (i.e. Isparta Angle) ensuring proper resolution of major fast and slow anomalies in the upper mantle.

To assess what fraction of the actual perturbation amplitudes can be retrieved in the resolved model, we carried out realistic amplitude recovery tests. These tests also provided us with additional means for assessing the robustness of the dipping Aegean and Cyprean fast anomalies. We used a synthetic input model space having exactly the same properties and parameters (i.e. size, number of nodes) as the model used in actual inversions. We introduced dipping fast perturbation patterns similar to the resolved Aegean and the Cyprean anomalies in this synthetic model (Figs 8a1 and a2, respectively). We assigned fixed +3 per cent perturbation amplitudes to these anomalies throughout the model. Using exactly the same governing forward problem as our actual tomographic problem, we calculated artificial traveltime residuals and used these residuals in the synthetic inversion. Figs 8(b1–b3) summarizes the results of these recovery tests, which show that our data set, model parametrization and inverse problem setup can successfully retrieve the general outline of the input synthetic anomalies. The general mean of the recovered amplitudes is +1.5 per cent, which is half of the input synthetic perturbation. The mean of the recovered amplitudes for the Aegean (Figs 8b1 and b3) and the Cyprean anomalies (Figs 8b2 and b3) are +1.4 and +1.6 per cent, respectively. We attribute this difference to the fact that the Aegean anomaly is located towards the western edge of the model and hence is relatively less well sampled. These types of recovery tests are useful for inferring actual amplitudes of real resolved structures. However, one must keep in mind that such a proxy is limited by the aforementioned basic tomographic assumptions and the character of the inversion algorithm.

4 DISCUSSION

In this section we interpret the robust features of our tomographic model and discuss how the resolved upper-mantle structures might be related to the different tectonic deformation styles and associated tectonic provinces across Anatolia. We conclude the discussion with an evolutionary scenario, with constraints on timing from regional geological investigations.

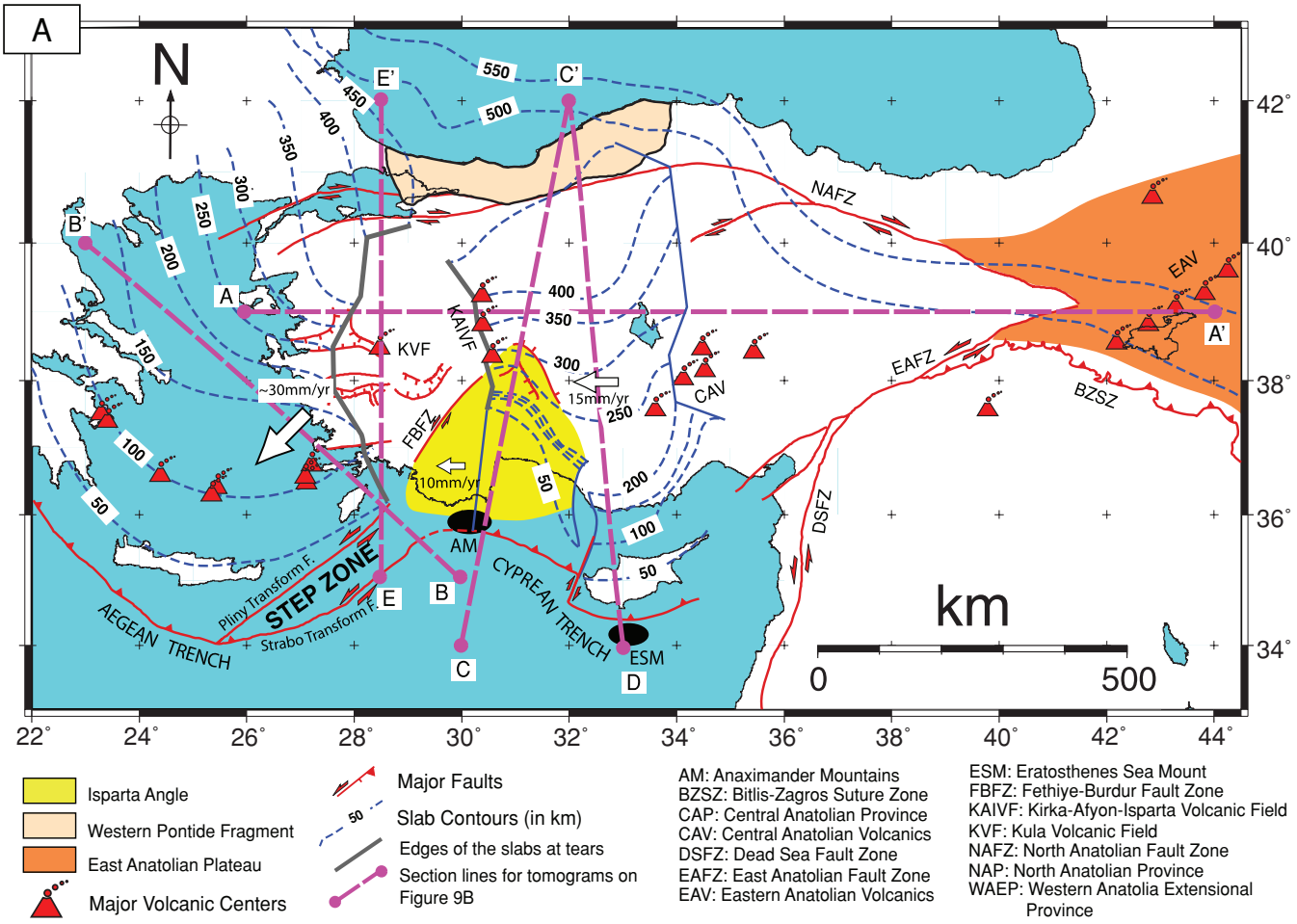

Figure 9. (A) General map of the study area with inferred contours (in km) of the Aegean and the Cyprean slabs, tectonic provinces, major structural and geological features. The dashed magenta lines show locations of cross-section shown in Fig. 9(B). The slab contours are plotted by tracing the approximate upper edges/surfaces of the Aegean and Cyprean fast anomalies in our tomograpic model. (B) Interpretation of the tomographic images along multiple sections across Anatolia. See inset in Fig. 9(A) for abbreviations. Small open circles are earthquake hypocentres ($M_w \geq 4.0$) for the period 1900–2010 acquired from European Mediterranean Seismological Center and Kandilli Observatory and Earthquake Research Institute catalogues. Topographic profiles with 10× vertical exaggeration are also shown at the top of cross-sections.

4.1 The slabs

The most prominent structures in our tomography model are the fast anomalies located to the north of the Cyprean and Aegean trenches. Based on their vertical extents and relationships with the associated trenches, we interpret these structures as segments of the subducting African oceanic lithosphere (Fig. 9B, cross-sections B'–B, C–C' and D–C′). The fast anomaly associated with the Aegean trench has also been detected by Spakman *et al.* (1988), Bijwaard *et al.* (1998), Piromallo & Morelli (2003) and Chang *et al.* (2010) using traveltime tomography, and interpreted as the subducting oceanic lithosphere of Africa (hereafter referred to as 'the Aegean slab') beneath the Aegean basin and Western Anatolia (Fig. 9B, B'–B). However, none of these studies were able to clearly resolve the fast anomaly associated with the Cyprus trench (hereafter referred to as 'the Cyprus slab') (Faccenna *et al.* 2006). Our tomographic cross-sections across this structure indicate that the Cyprus slab is subvertical at depths shallower than 200 km and begins dipping northward with a ∼45° angle at depths between 200 and 400 km (Fig. 9B, C–C′). Below 400 km, the dip of the slab becomes much gentler and it begins to flatten out, suggesting that it lies flat on the 660 km mantle transition zone (Fig. 9B, D–C′). The Cyprus slab terminates rather sharply at the tip of the Isparta Angle in the west and along 34°–35° longitude in the east (Fig. 9A). Our tomograms also indicate that the lateral continuity of the Cyprus slab is disrupted by a minor northeastward offset or tear at shallow depths (<200 km), west of Cyprus (Figs 9A and 10). This right-lateral tear aligns with the dextral Paphos transform fault on the surface (Fig. 1), which is associated with intermediate depth seismicity (Engdahl *et al.* 1998; Papazachos & Papaioannou 1999; Pilidou *et al.* 2004; Papadimitriou & Karakostas 2006; Wdowinski *et al.* 2006).

Our tomograms show that the Aegean slab and the Cyprus slab are clearly separated from each other (Figs 6a–f and Fig. 9A). The Aegean slab has its eastern termination at the north part of the Pliny and Strabo trenches/transforms (Figs 1 and 9A). In this region, it dips northwestward with an angle of ∼45° (below 100 km), but the dip direction changes to N and NE towards its western parts. Hence, the slab defines a roughly northward-concave configuration (Fig. 10). The western portions of this slab beneath the central

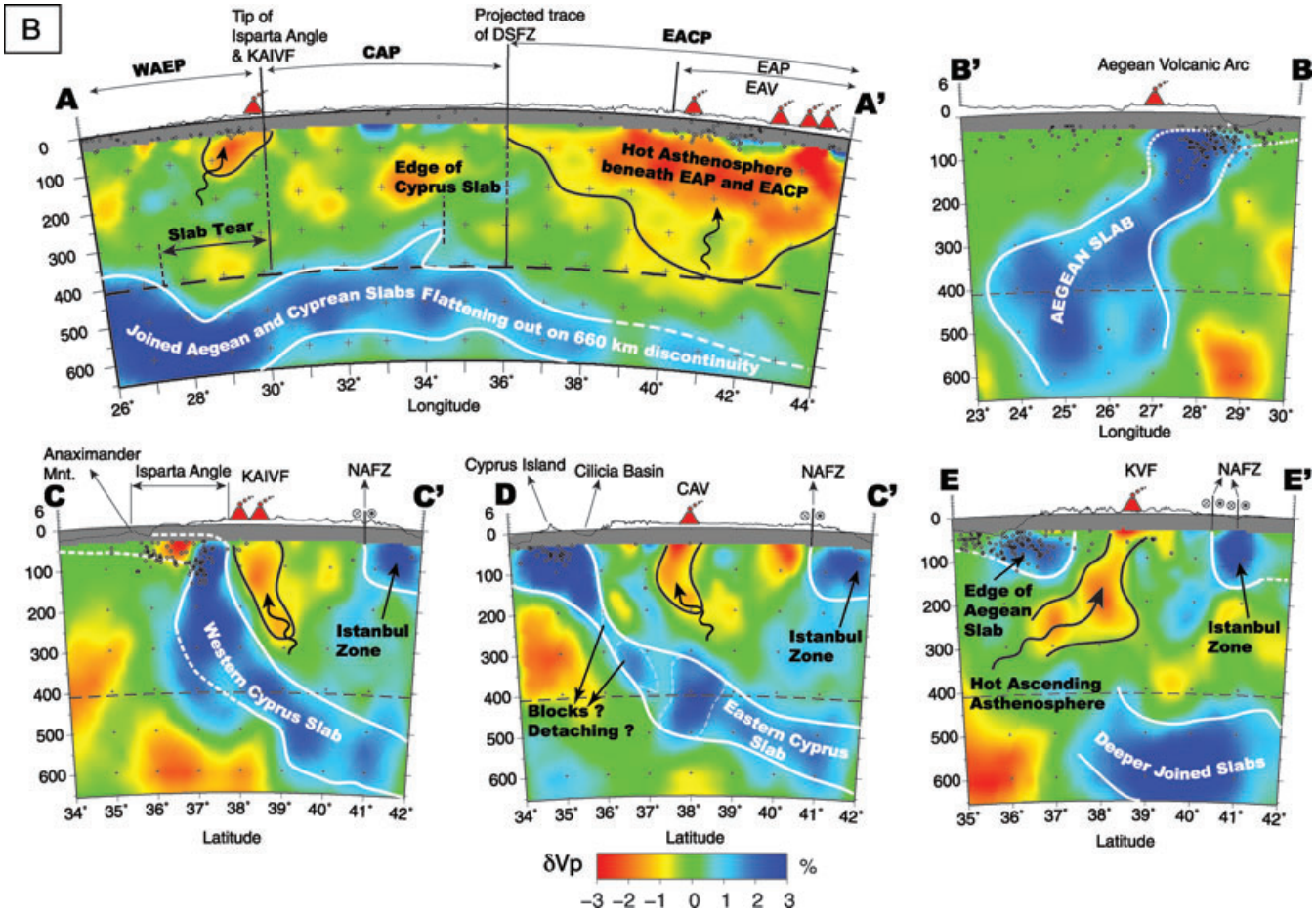

Figure 9. (*Continued.*)

Aegean Sea are located at the edge of our tomographic model and are poorly resolved. The eastern parts that remain beneath Anatolia, however, are better resolved.

The seismic anisotropy and dynamics of the upper mantle in the eastern Mediterranean region was investigated in various studies (Hatzfeld *et al.* 2001; Sandvol *et al.* 2003; Schmid *et al.* 2004; Şapaş & Boztepe-Guney 2009; Biryol *et al.* 2010). Many of these studies examined the relationships between the Aegean subduction roll-back related crustal strain-field and observed pattern of mantle anisotropy. In their recent study, Biryol *et al.* (2010) argued that the SW roll-back of the Aegean Slab could be responsible for the consistent NE–SW pattern of anisotropy/asthenospheric-flow underneath the north-central Anatolia. The observed configuration of the Aegean slab in our tomographic model is in accord with this interpretation. However, the lack of shear wave splitting observations from southern and central Anatolia makes further interpretations difficult regarding the effects of the Cyprus slab and the gap between the two slabs.

The fast anomalies associated with the Aegean slab and the Cyprus slab merge at depths of ∼500 km to form a coherent, gently dipping or nearly flat lying fast anomaly beneath Anatolia (Fig. 9B, A–A′). Previous larger-scale seismic tomography studies in the region resolved this broad and flat anomaly as well (Spakman 1985; Bijwaard *et al.* 1998; Piromallo & Morelli 2003). This is probably associated with the upper-mantle phase transition at 660 km that obstructs the penetration of the subducting lithosphere into the deeper mantle. This anomaly is also observed in receiver function results of Özacar *et al.* (2008) and in tomography models of Bijwaard *et al.* (1998), who indicate that it follows the palaeotrace of the Tethyan ocean and continues to the southeast beneath the Himalayan orogen (at depths of 500–1400 km) (see also Hafkenscheid *et al.* 2006).

The mean fast velocity perturbations associated with the Cyprus and the Aegean slabs are ∼+1.7 per cent (Fig. 9B, B′–B, C–C′ and D–C′). Our amplitude recovery test showed that the inversion achieves a ∼50 per cent recovery of the actual anomaly amplitudes, so the expected actual amplitudes of the perturbations associated with these slabs are ∼3.4 per cent. This velocity perturbation is comparable to the perturbations on the order of 3–4 per cent observed for old subduction zones such as Izu-Bonin, Tonga, Japan, Kuril (Deal & Nolet 1999; Deal *et al.* 1999) and agrees well with the Mesozoic age (>100 Ma) of the subducting African lithosphere (van Hinsbergen *et al.* 2005).

The fast velocity perturbations on the order of ∼1.6 per cent located in the northwest part of the study area (Fig. 9B, C–C′, D–C′ and E–E′) are probably associated with the thicker and older lithosphere of the northern Anatolian province (Figs 1 and 9A). This region is characterized by intensely deformed, imbricated Precambrian to Late Paleozoic basement of the so-called Eastern and Western Pontides, which represent the accreted continental terrains during the Cimmerian orogeny (Bozkurt 2001). Although this region is located at the northern edge of our tomographic model, the resolution here is good enough, particularly at the western and eastern ends, owing to the denser station coverage. We interpret the fast anomalies located to the west of north Anatolia as thick lithospheric

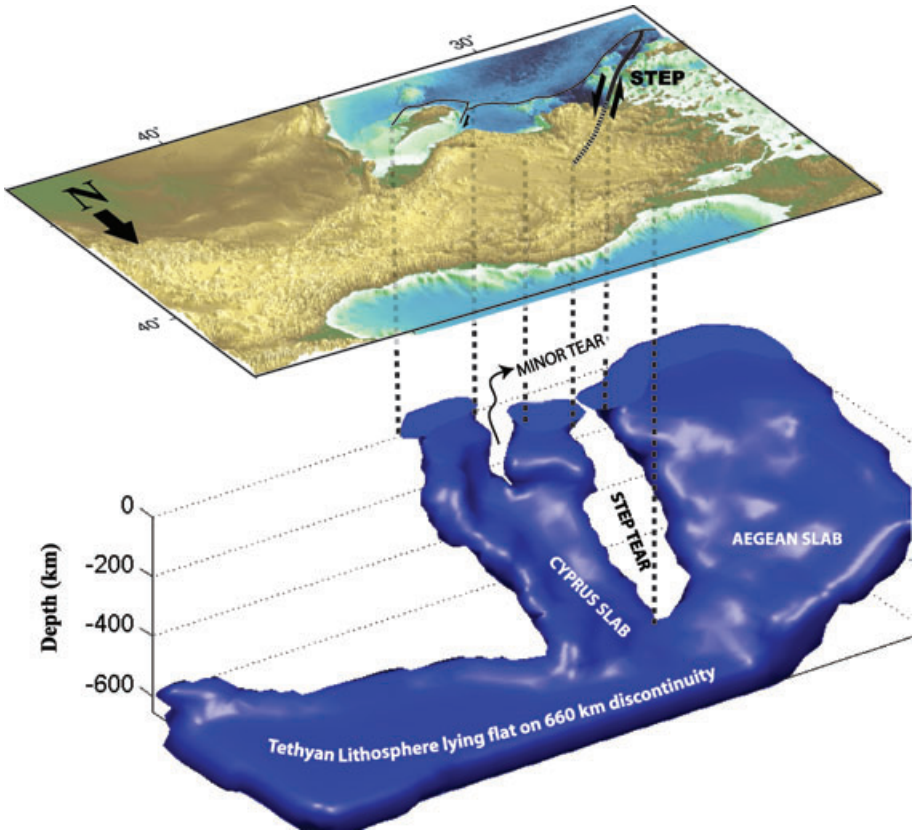

Figure 10. 3-D diagram of the resolved segmented geometry of the subducting African lithosphere beneath Anatolia inferred from our tomographic model. The isosurfaces for this slab model are obtained by tracing the slab related and coherent fast anomalies with amplitudes larger than +1.5 per cent. Dashed, black lines shows the projected locations of the slab features on the surface (3-D map at top). Important structural features are shown both on the 3-D model and on the relief map.

mantle beneath the western Pontides (the regions labelled 'Istanbul Zone' on Fig. 9B, C–C', D–C' and E–E'). The thick lithosphere terminates abruptly at the southern block of the NAFZ at shallower depths (<100 km), whereas it exhibits some dipping structural complexity at depths between 100 and 200 km. In this respect, the NAFZ forms a rather sharp, lithospheric scale structural boundary between the older lithosphere of the north Anatolian province and the younger Central Anatolian province or Anatolian Plate. This implies that the NAFZ is a lithospheric scale transform fault, meaning the associated deformation extends through the entire crust and penetrates into the uppermost mantle, at least for its western segment. This observation agrees with the interpretation that the NAFZ follows the weakness zone associated with the northern sector of the Neotethyan suture(s) at the northern part of Anatolia (Bozkurt 2001; Şengör *et al.* 2005). Based on this result, our study is the first to resolve and interpret the deeper structure of the North Anatolian Fault. Similar observations exist for portions of the much older San Andreas Fault (SAF), which is thought to be analogous to the NAFZ. Zhu (2000) and Yan & Clayton (2007) observed a 6–8 km vertical offset of the Moho discontinuity across the SAF in southern California using *P*-wave receiver functions, and argued that the SAF extends through the entire crust for that segment. Using *P*-wave tomography, Benz *et al.* (1992) detected a velocity contrast following the strike of the SAF beneath its central segment.

In various studies (i.e. Dilek & Altunkaynak 2009; Dilek & Sandvol 2009) it is argued that the deeper section of the Cyprus slab is detached along a trench-parallel tear and the shallower attached portion is now dipping with a shallow angle at the eastern side of the Isparta Angle, generating the Quaternary Central Anatolia Volcanics (CAV) (Fig. 9a). Our tomographic images contradict the idea of a shallow dipping Cyprus slab with a deeper detached section. In this respect, the eastern sector of the Cyprus slab is too deep (∼250 km) beneath the CAV to explain the young volcanism there (Fig. 9B, D–C′), although, flow related to the sinking of the slab may play a role.

4.2 The tears and slab edges

Another robust feature of our tomographic model is the N–S trending slow velocity anomalies, with amplitudes in the order of −1.4 per cent, that extend from 60 km down to depths of 300 km between the Aegean and Cyprus slabs (Fig. 9B, A–A′ and E–E′). Various studies associated this region that is roughly defined by the Isparta Angle (and hence the western termination of the Cyprus slab) with a vertical tear within the northward subducting African lithosphere (Büyükaşıkoğlu 1979; Wortel & Spakman 1992; Barka & Reilinger 1997; Dilek & Altunkaynak 2009; Dilek & Sandvol 2009). Our tomographic model supports the idea of a vertical or subvertical tear between the Aegean and the Cyprus slabs that is now occupied by slow velocity perturbations (Figs 6a–f). This feature is also visible in tomographic models of Spakman *et al.* (1993) and Piromallo & Morelli (2003); De Bordeer *et al.* (1998) interpreted the slow anomaly pattern as vertically rising asthenosphere along a vertical tear in the subducting Aegean slab. Based on our tomography model, we support this interpretation. Our model shows that the tear might be subvertical, however, and it is between the

Cyprus and Aegean slabs, which are separated from each other with a left-lateral offset (slab contours on Fig. 9A). In addition, our tomograms show that the lateral extent of the tear spans nearly the entire width of the WAEP (Figs 6a–e and 9B, A–A′). In our tomographic model, the trends of the upwelling hot asthenosphere are located directly below the Kirka-Afyon-Isparta (KAIVF) and Kula Volcanic Fields (KVF) (Fig. 9B, A–A′ and C–C′). The KVF is associated with Pliocene–Pleistocene alkaline volcanism (Richardson-Bunbury 1996). Geochemical analysis by Gülen (1990) and Tokçaer *et al.* (2005) indicates that the volcanism in the region is associated with rapid upwelling of asthenosphere beneath western Anatolia. Similar to KVF, KAIVF is also associated with alkaline volcanism with a southward younging pattern of ages from Middle-late Miocene (∼17 Ma) to Pliocene (∼4 Ma) (Savaşçın & Oyman 1998; Dilek & Altunkaynak 2009). This southward younging pattern is interpreted in terms of propagation of the tear between the Cyprus and the Aegean slabs (Dilek & Altunkaynak 2009). In brief, our tomographic images clearly show the geometry of this inferred tear between the Cyprus and Aegean slabs and the upwelling hot asthenosphere through it (slab contours on Figs 9A and 9B, A–A′, C–C′ and E–E′).

Our tomographic model shows an abrupt eastern termination of the Cyprus slab along the zone defined by the 33–34°E longitudes (Figs 6c–f and 9B, A–A′). To the east of this zone, we observe a relatively homogeneous slow velocity anomaly beneath the EAP and the collisional Neogene volcanics of East Anatolia starting east of 35–36°E longitude (Figs 6a–e, 7d–f and 9B, A–A′). The mean velocity perturbation associated with this anomaly is approximately −1.5 per cent and it extends as deep as 400 km beneath the EAP. This slow velocity anomaly is resolved in various studies using different techniques (Al-Lazki *et al.* 2003; Lei & Zhao 2007; Gans *et al.* 2009) and it is associated with the asthenosphere that ascended and was emplaced beneath the plateau after the detachment of the northward subducting Arabian oceanic lithosphere (Keskin 2003; Şengör *et al.* 2003). Our model clearly outlines the 3-D extent of this hot, buoyant asthenospheric body that is believed to be supporting the relatively thin crust of this ∼2 km high plateau (Şengör *et al.* 2003; Zor *et al.* 2003; Özacar *et al.* 2008, 2010b). The volcanism associated with the EAP shows various compositional characteristics. It is calc-alkaline and old in the north (11 Ma) and alkaline and younger in the south (∼2.0 Ma). Keskin (2003) argued that the subduction component of the volcanics decreases from north to south, in the later phases of the volcanism. This is in agreement with our tomograms for this region, where we observe the largest volumes of highest amplitude slow perturbations in the southern parts of the EAP (Figs 7d and 9B, A–A′). Our tomograms also show that the eastern termination of the Cyprus slab (the eastern edge of the subducting African lithosphere) and the western tip of the emplaced asthenosphere nearly align with the boundary between EACP to the east and CAP to the west (Figs 9A and 9B, A–A′). This is in good agreement with P_n velocity observations of Gans *et al.* (2009) and tomography results of Lei & Zhao (2007).

The western extent of the EACP roughly aligns with the northward projection of the Dead Sea Transform Fault (Barka & Reilinger 1997) (Figs 9A and 9B, A–A′). This fault marks the plate boundary between Africa and Arabia. In an earlier study, Reilinger *et al.* (1997) argued that the crust of Eastern Anatolia is hot and weak due to the presence of hot buoyant asthenosphere beneath the region (Keskin 2003). Hence, it is this weak crust that accommodates the N-S convergence between Eurasia and Arabia and defines the extent of the EACP. This is in agreement with the distribution of the slow anomalies in our tomographic model. Indeed, the western edge of the slow anomaly associated with Eastern Anatolia is roughly located along the EACP–CAP transition zone and aligns with the northward projection of the Dead Sea Transform Fault (Fig. 9A). In Western Anatolia, the northern tip of the Isparta Angle defines the boundary between WAEP and CAP. Similar to the EACP case explained above, Dilek & Altunkaynak (2009) argued that the strength of the crust is relatively low in the Western Anatolia province due to postcollisional magmatism, in agreement with high heat flow values measured in this region (İlkışık 1995). Hence the weaker crust of western Anatolia is probably responsible for the distributed extension in WAEP compared to the relatively slowly deforming CAP (Aktuğ *et al.* 2009). Our tomographic model shows that WAEP is underlain by a wide tear that is occupied by hot, upwelling asthenosphere. In fact, there is a remarkable spatial correlation between the eastern edge of the tear on our tomograms and the eastern limit of WAEP (Fig. 9A and 9B, A–A′). Based on these observations, our tomographic model indicates that the distribution of upper-mantle features such as slab tears, slab edges and upwelling hot asthenospheric volumes contribute to the distribution of the deformational domains throughout Anatolia.

Various geochemical studies focusing on the CAV and the composition of the associated volcanics indicate a clear subduction component (Kuşçu & Geneli 2010 and references therein). As discussed earlier, the location of the Cyprus slab is too deep (>200 km) to be the direct cause of the volcanism here (Fig. 9B, D–C′). If subduction is responsible for this volcanism, perhaps the dip of the slab was shallower during Eocene–Early Miocene time, when a major phase of calc-alkaline volcanism took place in this province (Savaşçın & Oyman 1998). The current location of the resolved western Cyprus slab and its dip imply that the slab rolled southwards between Early Miocene to present. Alternatively, some studies associate the calc-alkaline volcanism in this region with post-collisional processes (Druitt *et al.* 1995; Notsu *et al.* 1995). In contrast, recent studies indicated that the late stage (Pliocene-Pleistocene) volcanism in the region is associated with alkaline basalts having an asthenospheric source with no subduction-related geochemical signature (Aydın 2008). On our tomograms, the region defined as the CAV is directly underlain by slow velocity perturbations on the order of 1–2 per cent that extend as deep as 200 km (Fig. 9B, D–C′). It is possible that these slow anomalies are due to the presence of ascending, hot, buoyant asthenosphere containing partial melts, which are responsible for the volcanism in the CAV. Although the current outline of the Cyprus slab and the slow anomalies may favour a dominantly asthenospheric source for the latest phase of volcanism in the region, in accord with results of Aydın (2008), a contribution from the subduction of the Cyprus slab cannot be ruled out based on its close proximity to the ascending asthenosphere. Hence, this configuration might explain the mixed characteristics of volcanism (calc-alkaline to alkaline) observed in the CAVP (Kuşçu & Geneli 2010). Perhaps, the earlier shallow dip of the Cyprus slab beneath central Anatolia shielded this province from large volumes of upwelling asthenosphere and consequently contributed to its higher crustal strength and lower internal deformation (Allmendinger *et al.* 2007; Aktuğ *et al.* 2009). The presence of the Cyprus slab may also account for the more gradational transition from N–S contraction in the east to N–S extension in the west.

4.3 Evolution

We now address the question of how the observed upper-mantle structures evolved into their present configuration. This question has been extensively addressed for the Eastern Anatolia region (Keskin

2003; Şengör *et al.* 2003). Hence we will mainly focus on the evolution of the Cyprus and the Aegean slabs beneath the central and western Anatolia.

In a recent study Govers & Wortel (2005) pointed out that slab edges and associated tearing of subducting lithosphere along horizontal terminations of subduction trenches (transform faults) are commonly observed in the Mediterranean region. They termed these kinks in plate boundaries as Subduction Transform Edge Propagator (STEP). Govers & Wortel (2005) also argued that a STEP zone exists in the subducting African lithosphere between the Aegean and the Cyprean trenches defined by the left-lateral Pliny and Strabo transforms. They associated the formation of the STEP zone with the differential trench retreat rates where the retreat is in an SW direction and much faster for the Aegean trench ($\sim$30 mm yr^{-1}) compared to the central Cyprus trench ($<$10 mm yr^{-1}) (McClusky *et al.* 2003; Wdowinski *et al.* 2006). Our tomograms show a clear separation between the edges of the Cyprus and the Aegean slabs both in shallower and deeper parts of the model ($<$500 km) (Figs 9A and 10). We believe the mechanism associated with this gap is dynamically related to the initiation and propagation of the tear between the rapidly SW retreating Aegean slab and the relatively static Cyprus slab. The widest part of the tear is located at depths between 250 and 350 km beneath the oldest volcanics of the KAIVF (Figs 6d and e and 9A). This argues that the tear may have initiated at a deeper part of the subducting African lithosphere beneath the northern tip of KAIVF and propagated in both down-dip (North) and up-dip (South) directions while the Aegean slab rapidly retreated to the SW. In this respect, the configuration of the Aegean and the Cyprus slabs supports the existence of a STEP zone and associated slab tear between the Aegean and the Cyprus slabs. Dilek & Altunkaynak (2009) also associated the zone marked by the tip of the Isparta Angle with a STEP related tear within the subducting African lithosphere based on the distribution of alkaline volcanism in this region. Our tomographic model is the first to show the subsurface STEP tear geometry with a high resolution in 3-D (Fig. 10).

It is also important to address the initial causes of the observed differential retreat rates between the Cyprean and the Aegean trenches. In a recent review, Wortel *et al.* (2009) argued that STEP faulting could occur in a case where subduction is obstructed as continental crust enters into the trench. Recent active source surveys by Netzeband *et al.* (2006) showed that the crust that is currently entering the Cyprean trench is actually the thinned continental margin of the African Plate. This could explain the obstruction or slowing-down of the subduction/trench retreat along the entire length of the Cyprus trench and STEP formation at its western margin where it meets the Aegean slab.

The configuration of the Cyprus slab in the region of the Isparta Angle is rather complex. Our model shows that the steeply dipping section of this slab between depths of 60 and 200 km is located near the northern edge of the Isparta Angle (Fig. 9B, C–C′). This is also supported by the presence of intermediate depth seismicity (70–120 km deep) in this region (Figs 9A and B, C-C′). The resolution of the model is poor at shallower depths owing to the subvertical incidence angle of the teleseismic rays. Consequently, we can only infer the location and configuration of the subducting lithosphere above 60 km based on the position of the trench. Various studies have stated that the junction of the Aegean and the Cyprean trenches is at the cusp south of the Anaximander Mountains, offshore from southwestern Anatolia (Zitter *et al.* 2003; ten Veen *et al.* 2004; Aksu *et al.* 2009, Fig. 9A). If this is roughly the location of the tip of the Cyprus Subduction Zone where the African lithosphere begins to dip beneath southwestern Anatolia, then it should be dipping NNE at fairly shallow angles until it reaches the tip of the Isparta Angle, where it becomes steeper (Fig. 9B, C–C′). The distributed intermediate depth seismicity in the zone of Isparta Angle might be related to this configuration. In addition, receiver function analysis for station ISP located in this region indicates fairly thick crust ($\sim$42 km) with a rather complex structure (Zhu *et al.* 2006; Erduran 2009). Thus, the shallow dip of the subducting lithosphere might be due to a subducted impediment that is similar to the Eratosthenes Seamount located at the eastern segment of the subduction zone (Fig. 1). Eratosthenes Seamount has been shown to be a continental fragment of the African Plate embedded in attenuated continental crust of the African margin (Robertson 1998; Netzeband *et al.* 2006). The anticlinal core/bulge of the Anaximander Mountains (ten Veen *et al.* 2004) might be the surface expression of such a deep seated, locally thicker crust subducting beneath the Isparta Angle. This is in agreement with studies by Rotstein *et al.* (1985), Poisson *et al.* (2003) and Robertson *et al.* (2009), who argued that earlier phases of segregated plateau/platform subduction/accretion might play an important role in the current configuration of the Isparta Angle. The subduction of such an impediment may also explain the tight curvature of the Cyprus slab and the presence of a minor tear in between its western and eastern segments at shallow depths (Fig. 10). Barka & Reilinger (1997) argued that the zone defined by the Isparta Angle acts as an obstacle to the westward motion of central Anatolia. They based their argument on the slower westward motion of the Isparta Angle (10 mm yr^{-1}) with respect to the faster moving (15 mm yr^{-1}) southern Central Anatolia Province, where western Anatolia is moving SW with a much higher rate ($\sim$30 mm yr^{-1}, Fig. 9A). The presence of the obstructed, shallow subduction beneath this zone might argue for the blockage of the westward motion of southern central Anatolia. This 'backstop' effect can also explain the relatively slower motion of the Isparta Angle. This implies that the crustal deformation regimes observed in the Central Anatolian province and the Isparta Angle are possibly influenced by the obstructed, shallow subduction along the western segment of the Cyprus Subduction Zone.

In an earlier study, Wortel & Spakman (2000) argued that the continental collision or obstruction of subduction is a viable mechanism for slab steepening and detachment. In a recent study, Nolet (2009) pointed out that there is now increasing evidence supporting the complexity of slab detachment processes and that slabs may actually detach in the form of multiple fragments, rather than as a single piece. The Cyprus slab appears thinner, with various downdip separated segments at its eastern parts between depths of 130–400 km (Fig. 9B, D–C′). This 'blocky' appearance of the eastern portion of the Cyprus slab may be another example for complex detachment processes. Hence, we argue that the eastern segment of the Cyprus slab is in an early detachment phase. In addition, we think that the relatively low tectonic and seismic activity along the Cyprean trench (Bozkurt 2001; Pilidou *et al.* 2004; Papadamitriou & Karakostas 2006; Wdowinski *et al.* 2006) and the subvertical geometry of the slab argues for stagnation of the subduction of the Cyprus slab, and hence, a terminal-stage of subduction and early stage of detachment.

The detailed explanation of how and when the individual features of the structural model of the African lithosphere subduction evolved in this region needs further investigation and is beyond the scope of this paper. We can give a general outline and a time frame for the evolution, however, based on the robust features of our model and various geological observations in the region. As discussed earlier, our tomography results support the idea of STEP

faulting and STEP-related tear formation between the Aegean and the Cyprus trenches/slabs (Fig. 10). Various studies show evidence of changes in deformation styles, trends and principle stress fields in the vicinity of Isparta Angle beginning Late Miocene–Early Pliocene (∼7–5 Ma). The observations for the majority of these studies come from structural analysis of onshore and offshore basins and depocentres in the vicinity of Isparta Angle (e.g. Cilicia and Antalya Basins on Fig. 1, Poisson *et al.* 2003; ten Veen *et al.* 2004; Aksu *et al.* 2005, 2009; Alçiçek *et al.* 2005; İşler *et al.* 2005; Verhaert *et al.* 2006; Özel *et al.* 2007). In these studies, it is argued that beginning from Late Miocene–Early Pliocene, the stress regime in southern–southwestern Anatolia changed, overprinting earlier structures by extensional and transtensional structures. We believe this modification of the regional stress field is associated with the STEP fault/tear formation between the Aegean and the Cyprus slabs and gradual release of accumulated strain in the region due to differential retreat rates between the eastern and western segments of the African subduction zone prior to its segmentation. This interpretation for the timing of the STEP faulting/tear overlaps with the timing of the latest phase of volcanism located at the tip of the Isparta Angle (Kirka–Afyon–Isparta zone) and central western Anatolia (Kula region) (Savaşçın & Oyman 1998; Tokçaer *et al.* 2005; Dilek & Altunkaynak 2009). The current slab geometry and independent geological observations from the surrounding region suggests that the western segment of the Cyprus Subduction Zone was obstructed, due to the subduction of a locally thicker continental fragment of the African Plate during Late Miocene–Early Pliocene. Consequently, STEP faulting/tearing initiated at this location (tip of Isparta Angle). This gave way to a reorientation of the stress field in the region, and the Cyprus slab begun to steepen and ultimately entered into the detachment phase. Indeed, this inferred age of detachment initiation agrees with the numerical modelling results from Wong A Ton & Wortel (1997), who calculated a 'slab breakoff time' of ∼4.9–5.0 Ma using a wide range of values for subducting plate thermal structure.

5 CONCLUSIONS

Our *P*-wave traveltime tomography results for the Anatolian region indicate the northward subducting African lithosphere is segmented beneath Anatolia. These segments define the Cyprus and Aegean slabs, which are separated by tears/gaps occupied by slow anomalies and are possibly associated with hot upwelling asthenosphere. Major slow perturbations located in our tomographic model underlie active volcanic centres of Anatolia (i.e. Kula, Central Anatolia, Eastern Anatolia). The steep and downdip segmented configuration of the Cyprus slab might be an indication that it is in the early detachment phase. We also observe a clear contrast in lithospheric thickness across the western segment of the NAFZ in our tomographic model to depths of 100–150 km. We believe this is associated with the relatively thicker older lithosphere of the western Pontides. This strong contrast argues for the NAFZ being a lithospheric scale fault extending through the entire crust and following the weak zone associated with the Neotethyan suture(s). In this respect, the results of our analysis contribute significantly to the understanding of the structure and deformation styles at depth along this nascent transform plate boundary.

We observe a remarkable spatial correlation between the location of slab tears, associated hot ascending asthenosphere, and distribution of tectonic provinces across the entire region. Particularly, the subvertical and relatively continuous subduction along the Cyprean trench plays a key role in this framework. We suggest the presence of a continuous cold Cyprus slab underneath the Central Anatolia has a thermal shielding effect on the region and is an important influence on the relatively undeformed crustal characteristics of this province.

Based on the resolved configuration of slab segments, we favour a STEP model (Govers & Wortel 2005) for the segmentation and hence tear formation/migration between the Aegean and the Cyprus slabs. The generation of this STEP geometry is probably related to differential retreat rates between the Cyprean and the Aegean trenches that initiated when the attenuated continental margin of the African Plate entered into the Cyprean trench. Geological and structural records of changes in the stress field during Late Miocene–Early Pliocene in the vicinity of the Isparta Angle may be related to this STEP formation. We suggest the inferred gentle dip of the western Cyprus slab at shallow depths (<60 km) beneath Isparta Angle is related to subduction of a locally thicker continental fragment of the African margin, similar to the Eratosthenes Seamount further east. This continental fragment may have obstructed the subduction near the Isparta Angle and slowed the westward motion of southern Anatolia.

ACKNOWLEDGEMENTS

The authors thank Brandon Schmandt and Gene Humphreys of the University of Oregon for providing the teleseismic tomography code used in this study and for fruitful discussions on the interpretation of the seismic images. The seismic instrumentation for the NAF deployment was provided by the Incorporated Research Institutions for Seismology (IRIS) through the PASSCAL Instrument Center at New Mexico Tech to whom we thank. An important part of the data set is provided by National Earthquake Monitoring Center (NEMC) of Turkey. The remaining part of the data used in this study are provided by IRIS-DMC. The authors thank Nuretdin Kaymakçi and Douwe van Hinsbergen, Donna L. Whitney, Seda Yolsal and two anonymous reviewers for her helpful discussions and suggestions. The authors also thank Christine Gans for her help in editing the paper. This research was supported by NSF grant EAR0309838. Most of the figures were created using the Generic Mapping Tools (GMT) software (Wessel & Smith 1995).

REFERENCES

Aksu, A.E., Calon, T.J., Hall, J., Mansfield, S. & Yaşar, D., 2005. The Cilicia–Adana basin complex, Eastern Mediterranean: Neogene evolution of an active fore-arc basin in an obliquely convergent margin, *Mar. Geol.,* **221,** 121–159.

Aksu, A.E, Hall, J. & Yaltırak, C., 2009. Miocene-Recent evolution of Anaximander Mountains and Finike Basin at the junction of Hellenic and Cyprus Arcs, eastern Mediterranean, *Mar. Geol.,* **258,** 24–47.

Aktuğ, B. *et al*. 2009. Deformation of western Turkey from a combination of permanent and campaign GPS data: Limits to block-like behavior, *J. geophys. Res.,* **114,** B10404, doi:10.1029/2008JB006000.

Alçiçek, M.C., Kazancı, N. & Özkul, M., 2005. Multiple rifting pulses and sedimentation pattern in the Cameli Basin, southwestern Anatolia, Turkey, *Sediment. Geol.,* **173,** 409–431.

Al-Lazki, A., Seber, D., Sandvol, E., Türkelli, N., Mohamad, R. & Barazangi, M., 2003. Tomographic Pn velocity and anisotropy structure beneath the Anatolian plateau (eastern Turkey) and surrounding regions, *Geophys. Res. Lett.,* **30**, doi:10.1029/2003GL017391.

Allmendinger, R.W., Reilinger, R. & Loveless, J., 2007. Strain and rotation rate from GPS in Tibet, Anatolia, and the Altiplano, *Tectonics,* **26,** TC3013, doi:10.1029/2006TC002030.

Angus, D.A., Wilson, D.C., Sandvol, E. & Ni, J.F., 2006. Lithospheric structure of the Arabian and Eurasian collision zone in Eastern Turkey from S-wave receiver functions, *Geophys. J. Int.,* **166**(3), 1335–1346.

Aydın, M., Şahintürk, Ö., Serdar, H.S., Özçelik, Y., Akarsu, İ., Ungör, A., Çokuğraş, R. & Kasar, S., 1986. Ballıdağ-Çangaldağ (Kastamonu) arasındaki bölgenin jeolojisi, *Geological Society of Turkey Bulletin,* **29,** 1–16 (in Turkish with English abstract).

Aydın, F., 2008. Contrasting complexities in the evolution of calcalkaline and alkaline melts of the Nigde volcanic rocks, Turkey: textural, mineral chemical and geochemical evidence, *Eur. J. Mineral,* **20**(1), 101–118.

Barka A.A. & Reilinger R., 1997. Active tectonics of the Mediterranean region: deduced from GPS, neotectonic and seismicity data, *Annali di Geophis*., XI, 587–610.

Barka, A.A., Akyüz, S.H., Cohen, H.A. & Watchorn, F., 2000. Tectonic evolution of the Niksar and Tasova-Erbaa pull-apart basins, North Anatolian Fault Zone: their significance for the motion of the Anatolian block, *Tectonophysics,* **322,** 243–264.

Becel, A. *et al*., 2009. Moho, crustal Architecture and deep deformation under the North Marmara Trough, from the SEISMARMARA Leg 1 offshore-onshore reflection-refraction survey. *Tectonophysics,* **467,** 1–21.

Benz, H.M., Zandt G. & Oppenheimer, D.H., 1992. Lithospheric structure of northern California from teleseismic images of the upper mantle, *J. geophys. Res.,* **97,** 4791–4807.

Bijwaard, H., Spakman, W. & Engdahl, R., 1998. Closing the gap between regional and global travel time tomography, *J. geophys. Res.,* **103,** 30 055–30 078.

Biryol, C.B., Zandt, G., Beck, S.L., Özacar, A.A., Adıyaman, H.E. & Gans, R.C., 2010. Shear wave splitting along a nascent plate boundary: The North Anatolian Fault Zone, *Geophys. J. Int.,* **181,** 1201–1213.

Boray, A., Saroglu, F. & Emre, O., 1985. Isparta bolumunun Kuzey Kesminde D-B Daralma icin bazi veriler, *Jeoloji Mühendisligi,* **23,** 9–20 (in Turkish).

Bozkurt, E., 2001. Neotectonics of Turkey—a synthesis, *Geodin. Acta,* **14,** 3–30.

Bozkurt, E. & Koçyiğit, A., 1996. The Kazova basin: an active negative flower structure on the Almus Fault Zone, a splay fault system of the North Anatolian Fault Zone, Turkey, *Tectonophysics,* **265,** 239–254.

Büyükaşıkoğlu S., 1979. Eurasian-African plate boundary in Southern Turkey and Eastern Mediterranean, in *Proceedings of the 7th World Conference on Earthquake Engineering, Geoscience Aspects,* Istanbul, Turkey, part 1, 209.212.

Chang, S.J. *et al*., 2010. Joint inversion for three-dimensional S velocity mantle structure along the Tethyanmargin, *J. geophys. Res.,* **115,** B08309, doi:10.1029/2009JB007204.

Dahlen, F.A., Hung, S.-H. & Nolet, G., 2000. Frechet kernels for finite-frequency traveltimes, I. Theory, *Geophys. J. Int.,* **141,** 157–174.

Deal, M.M. & Nolet, G., 1999. Slab temperature and thickness from seismic tomography 2. Izu–Bonin, Japan, and Kuril subduction zones, *J. geophys. Res.-Solid Earth* **104,** 28 803–28 812.

Deal, M.M., Nolet, G. & Van Der Hilst, R.D., 1999. Slab temperature and thickness from seismic tomography 1. Method and application to Tonga, *J. Geophys. Res.-Solid Earth,* **104,** 28 789–28 802.

Dean, W.T., Monod, O., Rickards, R.B., Demir, O. & Bultynck, P., 2000. Lower Paleozoic stratigraphy and palaeontology, Karadere-Zira area, Pontus Mountains, northern Turkey, *Geol. Mag.,* **137,** 555–582.

De Boorder, Spakman, W., White, S.H. & Wortel, M.J.R., 1998. Late Cenozoic mineralization, orogenic collapse and slab detachment in the European Alpine Belt, *Earth planet. Sci. Lett.,* **164,** 569–575.

Delaloye, M. & Bingöl, E., 2000. Granitoids from western and northwestern Anatolia: geochemistry and modelling of geodynamic evolution, *Inter. Geol. Rev.,* **42,** 241–268.

Dewey, J.F. & Şengör, A.M.C., 1979. Aegean and surrounding regions: complex rnultiplate and continuum tectonics in a convergent zone, *Geol. Soc. Am. Bull.,* **90,** 84–92.

Dilek, Y. & Altunkaynak, S., 2009. Geochemical and temporal evolution of Cenozoic magmatism in western Turkey: mantle response to collision, slab break-off, and lithospheric tearing in an orogenic belt, *J. geol. Soc. Lond., Special Publications,* **311,** 213–233.

Dilek, Y. & Sandvol, E., 2009. Seismic structure, crustal architecture and tectonic evolution of the Anatolian-African Plate Boundary and the Cenozoic Orogenic Belts in the Eastern Mediterranean Region, *J. geol. Soc. Lond., Special Publications,* **327,** 127–160.

Druitt, T.H., Brenchley, P.J., Gökten, Y.E. & Francviglia, V., 1995. Late Quaternary rhyolitic eruptions from the central Turkey, *J. geol. Soc. Lond.,* **152,** 655–667.

Dumont, J,.F., Poisson, A. & Şahin A., 1979. Sur l'existence de coulissements senestres recents a l'extremite orientale de l'arc egeen (sud-ouest de la Turquie), *C. R. Acad. Sc. Paris,* **289,** 261–264.

Engdahl, E.R., Van Der Hilst, R.D. & Buland, R., 1998. Global teleseismic earthquake relocation with improved travel times and procedures for depth relocation, *Bull. seism. Soc. Am.,* **88,** 722–743.

Erduran, M., 2009. Teleseismic inversion of crustal S-wave velocities beneath the Isparta Station, *J. Geodyn.,* **47,** 225–236.

Faccenna, C., Jolivet, L., Piromallo, C. & Morelli, A., 2003. Subduction and the depth of convection in the Mediterranean mantle, *J. geophys. Res.,* **108**(B2), 2099, doi:10.1029/2001JB001690.

Faccenna, C., Bellier, O., Martinod, J., Piromallo, C. & Regard, V., 2006. Slab detachment beneath eastern Anatolia: a possible cause for the formation of the North Anatolian fault, *Earth planet. Sci. Lett.,* **242,** 85–97.

Gans, C.R., Beck, S.L., Zandt, G., Biryol, C.B. & Özacar, A.A. 2009. Detecting the limit of slab break-off in Central Turkey: new high-resolution *Pn* tomography results, *Geophys. J. Int.,* **179,** 1566–1572.

Glover, C. & Robertson, A.H.F., 1998. Role of extensional processes and uplift in the Plio-Quaternary sedimentary and tectonic evolution of the Aksu Basin, southwest Turkey, *J. geol. Soc., Lond.,* **155,** 365–368.

Govers, R. & Wortel, M.J.R., 2005. Lithosphere tearing at STEP faults: response to edges of subduction zones, *Earth planet. Sci. Lett.,* **236,** 505–523.

Gök, R., Türkelli, N., Sandvol, E., Seber, D. & Barazangi, M., 2000. Regional wave propagation in Turkey and surrounding regions, *Geophys. Res. Lett.,* **27,** 479–432.

Görür N., Oktay F.Y., Seymen I. & Şengör A.M.C., 1984. Palaeotectonic evolution of Tuzgölü basin complex, Central Turkey, in *The Geological Evolution of the Eastern Mediterranean,* vol. **17**, eds Dixon, J.E. & Robertson, A.H.F., *J. geol. Soc. Lond.*, Special Publication, pp. 81–96.

Görür N. *et al*., 1995. Rift formation in the Gökova region, southwest Anatolia: implications for the opening of the Aegean Sea, *Geol. Mag.,* **132,** 637–650.

Görür, N., Monod, O., Okay, A.İ., Şengör, A.M.C., Tüysüz, O., Yiğitbaş, E., Sakınç, M. & Akkök, R., 1997. Palaeogeographic and tectonic position of the Carboniferous rocks of the western Pontides (Turkey) in the frame of Variscan belt. *Bull. soc. Geol. France,* **168,** 197–205.

Gülen, L., 1990. Isotopic characterization of Aegean magmatism and geodynamic evolution of the Aegean subduction, in *Proceedings of the International Earth Science Colloquium on the Aegean Region,* Izmir, Turkey, Vol. 2, pp. 143–167.

Gürbüz, C. & Evans, J.R., 1991. A seismic refraction study of western Tuz Golu basin, central Turkey, *Geophys. J. Int.,* **106,** 239–251.

Gürbüz, C. & Üçer, B., 1980. Anadolu kavagında yapılan tas ocagı patlatmalarından elde edilen sismik kayıtların degerlendirilmesi, *Deprem Arastırma Bulteni (Turkey),* **49,** 39–49.

Hafkenscheid, E., Wortel, M.J.R. & Spakman, W., 2006. Subduction history of the Tethyan region derived from seismic tomography and tectonic reconstructions, *J. geophys. Res.-Solid Earth,* **111,** B08401, doi:10.1029/2005JB003791.

Hatzfeld, D. *et al*., 2001. Shear wave anisotropy in the upper-mantle beneath the Aegean related to internal deformation, *J. geophys. Res.,* **106,** 30 737–30 753.

Hung, S., Dalen, F. & Nolet, G., 2000. Frechet kernels of finite-frequency travel times—II. Examples, *Geophys. J. Int.,* **141,** 175–203.

İlkışık, M.O., 1995. Regional heat flow in western Anatolia using silica temperature estimates from thermal springs, *Tectonophysics,* **244,** 175–184.

İşler, F.I., Aksu, A.E, Hall, J., Calon, T.J. & Yaşar, D., 2005. Neogene development of the Antalya Basin, Eastern Mediterranean: an active forearc basin adjacent to an arc junction, *Mar. Geol.,* **221,** 299–330.

Jackson J.A., King G. & Vita-Finzi C., 1992. The neotectonics of the Aegean: an alternative view, *Earth planet. Sci. Lett.,* **61**(1992), 303–318.

Jackson, J., 1994. Active tectonics of the Aegean region, *Ann. Rev. Earth planet. Sci.,* **22,** 239–271.

Kalafat, D., Gürbüz, C. & Üçer, B., 1987. Investigation of the crust and upper mantle in the west of Turkey, *Deprem Arastirma Bulteni,* Istanbul **14**(59), 43–64 (in Turkish).

Kalafat, D., Yılmazer, M., Kekovalı, K. & Güneş, Y. 2008. Evolution Of Kandilli Observatory and Earthquake Research Institute (KOERI) Backbone Seismic Network, *Orfeus Observatory Co-ordination Meeting Abstracts,* Bacelona 2008.

Karahan, A.E. Breckmer H. & Baier B., 2001. Crustal structure at the western end of the North Anatolian Fault Zone from deep seismic sounding, *Annali di Geofisica,* **44,** 49–68.

Keskin, M., 2003. Magma generation by slab steepening and breakoff beneath a subduction–accretion complex: an alternative model for collision-related volcanism in Eastern Anatolia, Turkey, *Geophys. Res. Lett.,* **30,** 8046, doi:10.1029/2003GL018019.

Koçyiğit, A., 1991. An example of an accretionary forearc basin from northern central Anatolia and its implications for the history of subduction of Neo-Tethys in Turkey, *Geol. Soc. Am. Bull.,* **103,** 22–36.

Koçyiğit, A., 1996. Superimposed basins and their relations to the recent strike-slip fault zone: a case study of Refahiye superimposed basin adjacent to the North Anatolian Transform Fault, northeastern Turkey, *Int. Geol. Rev.,* **38,** 701–713.

Koçyiğit, A., Yılmaz, A., Adamia, S. & Kuloshvili, S., 2001. Neotectonics of East Anatolian Plateau (Turkey) and Lesser Caucasus: implication for transition from thrusting to strike-slip faulting, *Geodinamica Acta,* **14,** 177–195.

Kuşçu, G.G. & Geneli, F., 2010. Review of post-collisional volcanism in the Central Anatolian Volcanic Province (Turkey), with special reference to the Tepekoy Volcanic Complex, *Int. J. Earth Sci.,* **99,** 593–621.

Laigle, M., Becel, A., de Voogd, B., Hirn, A., Taymaz, T. & Ozalaybey, S., 2008. A first deep seismic survey in the Sea of Marmara: Deep basins and whole crust architecture and evolution, *Earth planet. Sci. Lett.,* **270**(3–4), 168–179.

Le Pichon, X. & Angelier, J., 1979. The Aegean arc and trench system: a key to the neotectonic evolution of the eastern Mediterranean area, *Tectonophysics* **6,** 1–42.

Lei, J. & Zhao D., 2007. Teleseismic evidence for a break-off subducting slab under Eastern Turkey, *Earth planet. Sci. Lett.,* **257,** 14–28.

Marquering, H., Dahlen, F.A. & Nolet G., 1999. Three dimensional sensitivity kernels for finite-frequency traveltimes: The banana-doughnut paradox, *Geophys. J. Int.,* **137,** 805–815.

McCallum J.E. & Robertson A.H.F., 1995. Late Miocene–Early Pleistocene Athalassa Formation, north central Cyprus: carbonate sand bodies in a shallow seaway between two emerging landmasses, *Terra Nova,* **7,** 265–277.

McClusky, S., Reilinger, R., Mahmoud, S., Ben Sari, D. & Tealeb, A., 2003. GPS constraints on Africa (Nubia) and Arabia plate motions, *Geophys. J. Int.,* **155,** 126–138.

McKenzie, D.P., 1978. Active tectonics of the Alpine–Himalayan belt: the Aegean Sea and surrounding regions, *Geophys. J. R. astr. Soc.,* **55,** 217–254.

Menke, W., 1989. *Geophysical Data Analysis: Discrete Inverse Theory, rev. ed.,* p. 285, Academic Press, San Diego, CA.

Netzeband, G.L., Gohl, K., Hubscher, C.P., BenAvraham, Z., Dehghani, G.A., Gajewski, D. & Liersch, P., 2006. The Levantine Basin crustal structure and origin, *Tectonophysics,* **418,** 167–188.

Nolet, G., 2009. Slabs do not go gently, *Science,* **324,** 1152–1153.

Notsu, K., Fujitoni, T., Ui, T., Matsuda, J. & Ercan, T., 1995. Geochemical features of collision related volcanic rocks in central and Eastern Anatolia, Turkey, *J. Volc. Geotherm. Res.* **64,** 171–192.

Örgülü, G., Aktar, M., Türkelli, N., Sandvol, E. & Barazangi, M., 2003. Contribution to the Seismotectonics of the Eastern Anatolian Plateau from Moderate and Small Size Events, *Geophys. Res. Lett.,* **30**(24) 8040, doi:10.1029/2003GL018258.

Okay, A.İ., 1996. Granulite facies gneisses from the Pulur region, Eastern Pontides, *Turkish J. Earth Sci.,* **5,** 55–61.

Özel, E., Uluğ, A. & Pekçetinöz, B., 2007. Neotectonic aspects of the northern margin of the Adana-Cilicia submarine basin, NE Mediterranean, *J. Earth Syst. Sci.,* **116**, 113–124.

Özacar, A.A., Gilbert, H. & Zandt., G., 2008. Upper mantle discontinuity structure beneath East Anatolian Plateau (Turkey) from receiver functions, *Earth planet. Sci. Lett.,* **269,** 426–434.

Özacar, A.A., Biryol, C.B., Zandt, G. & Beck, S.L., 2010a. *Deep Structure of Continental Strike-slip Faults Imaged by Receiver Functions,* European Geophysical Union General Assembly 2010; 02–07 May 2**010**, Vienna, Austria.

Özacar, A.A., Zandt, G., Gilbert, H. & Beck, S.L., 2010b. Seismic images of crustal variations beneath the East Anatolian Plateau (Turkey) from teleseismic receiver functions, *J. geol. Soc., Lond., Special Publications*, **340,** 485–496, doi:10.1144/SP34021.

Paige, C.C. & Saunders, M.A., 1982. LSQR: An algorithm for sparse linear equations and sparse least squares, *ACM Trans. Math. Soft.,* **8,** 43–71.

Pasquare, G., Poli, S., Venzolli, L. & Zanchi, A., 1988, Continental arc volcanism and tectonic setting in Central Anatolia, *Tectonophysics,* **146,** 217–230.

Pavlis, G.L. & Vernon, F.L., 2010. Array processing of teleseismic body waves with the USArray, *Comput. Geosci.,* **36,** doi:10.1016/j.cageo.2009.10.008/

Papadimitriou, E.E. & Karakostas, V.G., 2006. Earthquake generation in Cyprus revealed by the evolving stress field, *Tectonophysics,* **423,** 61–72.

Papazachos, B.C. & Papaioannou, C.A., 1999. Lithospheric boundaries and plate motions in the Cyprus area, *Tectonophysics* **308,** 193–204.

Piromallo, C. & Morelli, A., 2003. P wave tomography of the mantle under the Alpine-Mediterranean area, *J. geophys. Res.,* **108**(B2), 2065, doi:10.1029/2002JB001757.

Pilidou, S., Priestley, K., Jackson, J. & Maggi, A., 2004. The 1996 Cyprus earthquake: a large, deep event in the Cyprean Arc, *Geophys. J. Int.,* **158,** 85–97.

Poisson, A., Wernli, R., Sağular, E.K. & Temiz, H., 2003. New data concerning the age of the Aksu Thrust in the south of the Aksu valley, Isparta Angle (SW Turkey): consequences for the Antalya Basin and the Eastern Mediterranean, *Geol. J.* **38,** 311–327.

Price S. & Scott B., 1994. Fault block rotations at the edge of a zone of continental extension: southwest Turkey, *J. Struct. Geol.,* **16,** 381–392.

Reilinger R.E., McClusky S.C., Oral M.B., King W. & Toksöz M.N., 1997. Global Positioning System measurements of present-day crustal movements in the Arabia–Africa-Eurasia plate collision zone, *J. geophy. Res.,* **102**, 9983–9999.

Richardson-Bunbury, J.M., 1996. The Kula volcanic field, western Turkey: the development of a Holocene alkali basalt province and the adjacent normal-faulting graben, *Geol. Mag.,* **133,** 275–283.

Robertson, A.H.F. & Dixon, J.E., 1984. Introduction: aspects of the geological evolution of the eastern Mediterranean, in *The Geological Evolution of the Eastern Mediterranean,* pp. 1–74, Vol. 17, eds Dixon, J.E. & Robertson, A.H.F., J. Geol. Soc., London, Special Publications.

Robertson, A.H.F., 1994. Role of the tectonic facies concept in orogenic analysis and its application to Tethys in the Eastern Mediterranean region, *Earth Sci. Rev.,* **37,** 139–213.

Robertson, A.H.F. & Grasso, M., 1995. Overview of the late Triassic-Recent tectonic and palaeo-environmental development of the Mediterranean region, *Terra Nova,* **7,** 114–127.

Robertson, A.H.F., 1998. Tectonic significance of the Eratosthenes Seamount: a continental fragment in the process of collision with subduction zone in the eastern Mediterranean (Ocean Drilling Program Leg 160), *Tectonophysics,* **298,** 63–82.

Robertson, A.H.F., Poisson A. & Akıncı, Ö., 2003. Developments in research concerning Mesozoic-Tertiary Tethys and Neotectonics in the Isparta Angle, SW Turkey, *Geol. J.,* **38**(3–4), 195–234.

Robertson, A.H. F., Parlak, O. & Ustaömer, T., 2009. Melange genesis and ophiolite emplacement related to subduction of the northern margin of the Tauride–Anatolide continent, central and western Turkey, in *Collision and Collapse at the Africa–Arabia–Eurasia Subduction Zone,* pp. 9–66,

Vol. 311, eds van Hinsbergen, D.J.J., Edwards, M.A. & Govers, R., J. Geol. Soc., London, Special Publications.

Rotstein, Y. & Ben-Avraham, Z., 1985. Accretionary processes at subduction zones in the eastern Mediterranean, *Tectonophysics,* **112,** 551–561.

Sandvol, E., Seber, D., Barazangi, M., Vernon, F., Mellors, R. & Al-Amri A., 1998. Lithospheric seismic velocity discontinuities beneath the Arabian Shield, *Geophys. Res. Lett.,* **25**(15), 2873–2876.

Sandvol, E., Türkelli, N., Zor, E., Gök, R., Bekler, T., Gürbüz, C., Seber, D. & Barazangi, M., 2003. Shear wave splitting in a young continent-continent collision: An example from Eastern Turkey, *Geophys. Res. Lett.,* **30**(24), 8041, doi:10.1029/2003GL017390.

Şapaş, A. & Boztepe-Güney, A., 2009. Shear wave splitting in the Isparta Angle, southwestern Turkey: anisotropic complexity in the mantle, *J. Earth Syst. Sci.,* **118,** 71–80.

Saunders, P., Priestley, K. & Taymaz, T., 1998. Variations in the Crustal Structure Beneath Western Turkey, *Geophys. J. Int.,* **134,** 373–389.

Savaşçın, M.Y. & Oyman, T., 1998. Tectono-magmatic evolution of alkaline volcanics at the Kırka-Afyon-Isparta structural trend, SW Turkey, *Turkish J. Earth Sci.,* **7,** 201–214.

Schmandt, B. & Humphreys, E., 2010. Seismic heterogeneity and small-scale convection in the southern California upper mantle, *Geochem. Geophys. Geosyst.,* **11,** Q05004, doi:10.1029/2010GC003042.

Schmid, C., Van Der Lee, S. & Giardini, D., 2004, Delay times and shear wave splitting in the Mediterranean region, *Geophys. J. Int.,* **159,** 275–290.

Şengör, A.M.C., 1979. The North Anatolian transform fault, its age, offset and tectonic significance, *J. geol. Soc., Lond.,* **136,** 269–282.

Şengör, A.M.C. & Yılmaz, Y., 1981. Tethyan evolution of Turkey: a plate tectonic approach, *Tectonophysics,* **75,** 181–241.

Şengör, A.M.C., Yılmaz, Y. & Sungurlu, O., 1984. Tectonics of the Mediterranean Cimmerides: nature and evolution of the western termination of Palaeo-Tethys, in *The Geological Evolution of the Eastern Mediterranean,* pp. 119–181, Vol. 17, eds Dixon, J.E. & Robertson, A.H.F., J. Geol. Soc., London, Special Publications.

Şengör, A.M.C., Görür, N. & Şaroğlu, F., 1985. Strike-slip faulting and related basin formation in zones of tectonic escape: Turkey as a case study, in *Strike-slip Faulting and Basin Formation,* pp. 227–264., Vol. **37**, eds Biddle, K.T., Christie-Blick, N., Soc. Econ. Paleont. Miner. Spec. Publ.

Şengör, A.M.C., Özeren, S., Genç, T. & Zor, E., 2003. East Anatolian high plateau as a mantle supported, north-south shortened domal structure, *Geophys. Res. Lett.,* **30**(24), 8045, doi:10.1029/2003GL017858.

Şengör, A.M.C., Tüysüz, O., İmren, C., Sakınç, M., Eyidoğan, H., Görür, N., Le Pichon, X. & Claude Rangin, C., 2005, The North Anatolian Fault. A new look, *Ann. Rev. Earth planet. Sci.,* **33,** 1–75.

Seyitoğlu, G. & Scott, B., 1991. Late Cenozoic crustal extension and basin formation in west Turkey, *Geol. Mag.,* **128,** 155–166.

Seyitoğlu, G., Scott, B.C. & Rundle, C.C., 1992. Timing of Cenozoic extensional tectonics in west Turkey, *J. Geol. Soc., Lond.,* **149,** 533–538.

Spakman, W., 1985. A Tomographic Image of the Upper Mantle in the Eurasian-African-Arabian Collision Zone, *EOS,* **66,** p. 975.

Spakman, W.A.V., Wortel, M.J.R. & Vlaar, N.J., 1988. The Aegean subduction zone: a tomographic image and its geodynamic implications, *Geophys. Res. Lett.* **15,** 60–63.

Spakman, W.S., Van Der, Lee & Van Der, Hilst, 1993. Travel-time tomography of the European–Mediterranean mantle down to 1400 km, *Phys. Earth planet. Inter.,* **79,** 3–73.

Sodoudi, F. *et al*., 2006. Lithospheric structure of the Aegean obtained from P and S receiver functions, *J. geophys. Res.,* **111,** B12307, 1–23.

Taymaz T. & Price S.P., 1992. The 12.05.1971 Burdur earthquake sequence: a synthesis of seismological and geological observations, *Geophys. J. Int.,* **108,** 589–603.

Taymaz, T., Jackson, J. & Mckenzie, D.P., 1991. Active tectonics of the North and Central Aegean Sea, *Geophys. J. Int.,* **106,** 433–490.

Taymaz, T., Yılmaz, Y. & Dilek, Y., 2007a. The Geodynamics of the Aegean and Anatolia: Introduction, in *The Geodynamics of the Aegean and Anatolia,* pp. 1–16, Vol. 29, eds Tuncay, Taymaz, Yücel, Yılmaz & Yıldırım, Dilek, J. Geol. Soc., London, Special Publications.

Taymaz, T., Wright, T., Yolsal, S., Tan, O., Fielding, E. & Seyitoğlu, G., 2007b. Source Characteristics of June 6, 2000 Orta-Çankırı (Central Turkey) Earthquake: a synthesis of seismological, geological and geodetic (InSAR) observations, and internal deformation of Anatolian plate, *J. Geol. Soc., Lond., Special Publications*, **291,** 259–290.

ten Veen, J.H., Woodside, M., Zitter, T.A.C., Dumont, J.F., Mascle, J. & Volkonskaia, A., 2004. Neotectonic evolution of the Anaximander Mountains at the junction of the Hellenic and Cyprus Arcs, *Tectonophysics,* **391,** 35–65.

Tokçaer, M., Agostini, S. & Savaşçın, M., 2005. Geotectonic setting and origin of the Youngest Kula Volcanics (Western Anatolia), with a New Emplacement Model, *Turkish J. Earth Sci.,* **14,** 145–166.

Türkelli, N., Horasan, G., Kuleli, H.S. & Reiter, D., 1996. Preliminary results of velocity distribution study in eastern Turkey, *EOS, Trans. Am. Geophys. Un.,* **77**(46), p. 477.

Türkelli, N. *et al*., 2003. Seismogenic zones in Eastern Turkey, *Geophys. Res. Lett.,* **30,** 8039, doi:10.1029/2003GL018023.

Wessel, P. & Smith, W.H.F., 1995. New version of the generic mapping tools released, *EOS, Trans. Am. Geophys. Un.,* **76,** p. 329.

Wdowinski, S., Ben-Avraham, Z., Arvidsson, R. & Ekstrom, G., 2006. Seismo-tectonics of the Cyprian Arc, *Geophys. J. Int.,* **164,** 176–181.

Woodward, M.J., 1992. Wave-equation tomography. *Geophysics,* **57,** 15–26.

Wong A Ton, S.Y.M. & Wortel, M.J.R., 1997. Slab detachment in continental collision zones: an analysis of controlling parameters, *Geophys. Res. Lett.,* **24,** 2095–2098.

Wortel, M.J.R. & Spakman, W., 1992. Structure and dynamics of subducted lithosphere in the Mediterranean region, *Proc. K. Ned Akad Wet.,* **95,** 325–347.

Wortel, R. & W. Spakman, 2000. Subduction and slab detachment in the Mediterranean-Carpathian region, *Science,* **290,** 1910–1917.

Wortel, R., Govers, R. & Spakman, W., 2009. Continental collision and the STEP-wise evolution of convergent plate boundaries: from structure to dynamics, in *Subduction Zone Geodynamics,* pp. 47–59, eds Lallemand, S. & Funiciello, F., Springer Berlin Heidelberg, doi:10.1007/978-3-540-87974-9.

Van Hinsbergen, D.J.J., Hafkenscheid, E., Sakman, W., Meulenkamp, J.E. & Wortel, R., 2005. Nappe stacking resulting from subduction of oceanic and continental lithosphere below Greece, *Geology,* **33,** 325–328.

Verhaert, G., Similox-Tohon, D., Vandycke, S., Sintubin, M. & Muchez, P., 2006. Different stress states in the Burdur-Isparta region (SW Turkey) since Late Miocene times: a reflection of a transient stress regime, *J. Struct. Geol.,* **28,** 1067–1083.

Yan, Z. & Clayton, R., 2007. A Notch Structure on the Moho beneath the Eastern San Gabriel Mountains, *Earth planet. Sci Lett.,* **260,** 570–581.

Yılmaz, Y., 1990. Comparisons of the young volcanic associations of the west and the east Anatolia under the compressional regime: a review, *J. Volc. Geotherm. Res.,* **44,** 69–87.

Yılmaz, Y., Genç, Ş.C., Karacık, Z. & Altunkaynak, Ş., 2001. Two contrasting magmatic associations of NW Anatolia and their tectonic significance, *J. Geodyn.,* **31,** 243–271.

Zhao, L., Jordan, T. H. & Chapman, C.H., 2000. Three-dimensional Fréchet differential kernels for seismic delay times, *Geophys. J. Int.,* **141**: 558–576.

Zhu, L., 2000. Crustal structure across the San Andreas Fault, southern California from teleseismic converted waves, *Earth planet. Sci. Lett.,* **179,** 183–190.

Zhu, L., Mitchell, B., Akyol, N., Cemen, I. & Kekovali, K., 2006. Crustal thickness variation in the Aegean region and its implications for the extension of continental crust, *J. geophys. Res.,* **111**, doi:10.1029/2005JB003770.

Zitter, T.A.C., Woodside, J.M. & Mascle, J., 2003. The Anaximander Mountains: a clue to the tectonics of southwest Anatolia, *Geol. J.,* **38,** 375–394.

Zor, E., 2008. Tomographic evidence of slab detachment beneath eastern Turkey and the Caucasus, *Geophys. J. Int.,* **175,** 1273–1282.

Zor, E., Sandvol, E., Gürbüz, C., Türkelli, N., Seber, D. & Barazangi, M., 2003. The Crustal Structure of the East Anatolian Plateau from Receiver Functions, *Geophys. Res. Lett.,* **30,** 8044, doi:10.1029/2003GL018192.

SUPPORTING INFORMATION

Additional Supporting Information may be found in the online version of this article:

Appendices A–D. The material in this document provides additional results and explanations for our finite-frequency teleseismic *P*-wave tomography study. Here we present further statistical aspects of the data set, additional inversion results using various values for regularization parameters and altered versions of the data set.

Please note: Wiley-Blackwell are not responsible for the content or functionality of any supporting materials supplied by the authors. Any queries (other than missing material) should be directed to the corresponding author for the article.